nature communications

Article

https://doi.org/10.1038/s41467-025-63291-8

CFP1 promotes germinal center affinity maturation and restrains memory B cell differentiation through H3K4me3 modulation

Received: 15 January 2025

Accepted: 14 August 2025

Published online: 27 August 2025

Check for updates

Yanan Zhao[1,3], Shuoxu Gong[1,3], Yalin Yang[2], Yimiao Lu[1], Jingning Bai[1], Meiling Liu[1], Wanyu Bai[1,2] ✉ & Junchao Dong[1,2] ✉

Affinity maturation and differentiation of B cells in the germinal center (GC) are tightly controlled by epigenetically regulated transcription programs, but the underlying mechanisms are only partially understood. Here we show that *Cfp1*, an integral component of the histone methyltransferase complex Setd1A/B, is critically required for GC responses. *Cfp1* deficiency in activated B cells greatly impairs GC formation with diminished proliferation, somatic hypermutation and affinity maturation. Mechanistically, *Cfp1* deletion reduces H3K4me3 marks at a subset of cell cycle and GC-related genes and impairs their transcription. Importantly, *Cfp1* promotes the expression of transcription factors MEF2B and OCA-B and the *Bcl6* enhancer-promoter looping for its efficient induction. Accordingly, *Cfp1*-deficient GCB cells upregulate IRF4 and preferentially differentiate into plasmablasts. Furthermore, *Cfp1* ablation upregulates a panel of pre-memory genes with elevated H3K4me3 and leads to markedly expanded memory B populations. In summary, our study reveals that *Cfp1*-safeguarded epigenetic regulation ensures proper dynamics of GCB cells for affinity maturation and prevents the pre-mature exit from GC as memory cells.

Germinal centers (GC) are microstructures in the secondary lymphoid tissues where antigen-activated B lymphocytes undergo affinity maturation and terminal differentiation[1,2]. Antigen encounter activates B cell proliferation burst, leading to the formation of the dark zone (DZ) and light zone (LZ) of GC. In the DZ, GCB cells divide rapidly and accumulate mutations in the antibody variable regions that alter the affinity of BCR to antigens[3]. DZ B cells with functional BCR then shuffle to the LZ for competitive binding with and subsequent presentation of antigens to follicular helper T cells (Tfh) that favors B cell clones with higher affinity BCR. As a result, these LZ B cells obtain additional survival signals from T cells, which trigger the induction of c-Myc[4–6] and mTOR[7] expression for cell cycle entry and biomass synthesis, and are licensed to return to the DZ. Repeated rounds of proliferation and hypermutation followed by positive selection eventually leads to affinity maturation[1,2]. A small portion of LZ B cells that survive positive selection differentiate into memory B (MBC) and antibody-producing plasma cells (PC). The mechanisms that determine GCB fate from zonal cycling to terminal differentiation into effector cells are poorly understood.

Both extrinsic and intrinsic factors, including cytokines and transcription factors, have been shown to regulate GC commitment, affinity maturation and differentiation[3]. Interaction of activated cells

[1]Department of Immunology and Microbiology, Zhongshan School of Medicine, Sun Yat-sen University, Guangzhou, China. [2]Pediatric Hematology Laboratory, Division of Hematology/Oncology, Department of Pediatrics, The Seventh Affiliated Hospital of Sun Yat-Sen University, Shenzhen, China. [3]These authors contributed equally: Yanan Zhao, Shuoxu Gong. ✉e-mail: baiwy6@163.com; dongjch@mail.sysu.edu.cn

with cognate T cells and T cell-derived IL-4/IL-21 turn on key transcription factor *Bcl6*[8,9], which acts primarily as a transcription suppressor for an array of downstream target genes to instruct full commitment to a GC fate[10,11]. *Bcl6* also regulates the maintenance and terminal differentiation of GCB cells. For instance, *Bcl6* suppresses the expression of transcription factors HHEX[12], which has been shown to promote MBC differentiation, as well as cell migratory receptors EBI2 and S1PR1, which are critical for GC exit[13]. It is thus assumed that the on and off of *Bcl6* regulated transcription program coordinates memory B cell formation. In addition, mutual antagonism between BCL6 and PC-specific transcription factors IRF4 and BLIMP1 dynamically determines the fate choice between GCB cells and the differentiation into PCs[14,15].

While the GC-specific transcriptional circuits are relatively well understood, how epigenetic factors regulate the GC response remains largely unknown. As one of the most studied epigenetic modifications, histone H3K4 trimethylation (H3K4me3) predominantly marks active and poised promoters[16,17]. Despite positive correlations with gene expression suggested by prior studies mostly in early embryos and ES cells, whether H3K4me3 plays an instructive role in transcription is debatable and under intensive investigation[16,18], and the physiological roles of H3K4me3 in cell lineage differentiation are still unclear. The mammalian Setd1A/B histone methyltransferase complexes represent the major methyltransferase (HMT) activity for H3K4 trimethylation[16,17]. As an integral subunit of the complex, CFP1 has been shown to recruit Setd1A/B to unmethylated CpG islands to implement H3K4me3 marks[18–20] and is essential for the development of germ cells and multiple hematopoietic lineages[18,21–23].

In this study, we examine the roles of *Cfp1* on GC response and terminal B cell differentiation. Our work demonstrates that *Cfp1* is strictly required for GC entry, dynamics and affinity maturation through regulating GCB-related genes, including *Bcl6*. In addition, our data indicate that *Cfp1* prevents B cells from pre-maturely exiting the GC to differentiate into MBCs that is modulated by H3K4me3-mediated transcription.

Results

Cfp1 loss in mature B cells impairs activation and germinal center entry

To test the requirement for *Cfp1* in mature B cell development and response, we crossed mice carrying the $Cfp1^{flox}$ allele[24] with the $Cd21^{Cre}$ mice to delete *Cfp1* in transitional and mature B cells[25]. Early B cell development in the bone marrow of $Cfp1^{fl/fl}Cd21^{Cre}$ mice was unperturbed (Fig. S1A, B), and a reduction in the frequency but not the number of spleen follicular B cells (FOB) relative to $Cfp1^{fl/fl}$ control mice was observed (Fig. S1C, D). Meanwhile, both the frequency and the number of marginal zone B cells (MZB) were significantly increased by approximately threefold, suggesting that *Cfp1* promotes transitional B cell development in the spleen to FOB over MZB (Fig. S1C, D).

To investigate the role of *Cfp1* in antigen-specific B cell response, T cell-dependent antigen 4-hydroxy-3-nitrophenylacetyl (NP) conjugated to keyhole limpet hemocyanin (NP-KLH) in alum adjuvant was administrated to control and $Cfp1^{fl/fl}Cd21^{Cre}$ mice. In control mice, the frequency of $CD95^+GL7^+$ GC B cells gradually rose from 0.77% ± 0.26% at day 5 to 1.78% ± 0.46% at day 14 post immunization (p.i.) (Fig. 1A, B). The GCB frequency in $Cfp1^{fl/fl}Cd21^{Cre}$ mice was severely reduced by about 3-5-fold compared to $Cfp1^{fl/fl}$ mice at each time point (Fig. 1A, B). The GCB defect upon *Cfp1* deletion was reproducible with different adjuvants or antigens. When administrated with NP-KLH in manganese-based adjuvant (MnJ), an adjuvant that stimulates strong antibody responses[26], $Cfp1^{fl/fl}$ control mice showed 8.24% ± 1.56% GC B cells at 14 days p.i. and *Cfp1* ablation caused an over threefold reduction in GCB frequency (Fig. 1C). A similar degree of reduction in GCB frequency was also observed in mice immunized with sheep red blood cells (SRBC) (Fig. 1D). We next measured concentration of serum NP-specific antibodies at day 14 p.i. by ELISA. Compared with controls, total NP-IgM Abs were significantly reduced and NP-IgG1 Abs were nearly absent in $Cfp1^{fl/fl}Cd21^{Cre}$ mice (Fig. 1E). In addition, the $Cfp1^{fl/fl}Cd21^{Cre}$ mice were devoid of high affinity NP-specific Abs (Fig. 1F). We therefore concluded that *Cfp1* ablation in mature B cells led to significantly reduced germinal center B cells and drastically defective antibody affinity maturation.

The severe impairment of GC formation in the absence of *Cfp1* manifest from the early time points suggests that the $Cfp1^{fl/fl}Cd21^{Cre}$ B cells could be defective in GC entry. To test this, we examined the GC response as early as day 3 p.i. and the results showed that activated precursors ($IgD^-B220^+CD138^-GL7^+CD38^+$)[27,28] from $Cfp1^{fl/fl}Cd21^{Cre}$ mice were reduced by more than twofold than the controls (Fig. 1G), indicating impaired B cell activation. Assessing *Cfp1* deletion by genomic DNA digital droplet PCR and quantitative PCR indicated less efficient knockout of *Cfp1* in GCB cells recovered at day 14 p.i. than naive cells, suggesting potential counter selection of cells with efficient deletion from entering GC (Fig. S2A–C). In vitro Nojima culture[29] of the control and $Cfp1^{fl/fl}Cd21^{Cre}$ B cells on 40LB feeder cells for 4 days to mimic early GC response showed a significant reduction of $CD95^+GL7^+$ cells, confirming defects of *Cfp1*-deficient B cells in GC activation (Fig. 1H). The severely abrogated GC response and decreased activated precursors prompted us to explore the early stage of B cell activation upon antigen encounter. To this end, we stimulated naïve B cells from $Cfp1^{fl/fl}Cd21^{Cre}$ and control mice with CD40 antibody plus interleukin-4 (IL-4) and IL-21. Cell cycle analysis indicated that the ratio of cells in the G1 phase of cell cycle was significantly increased in $Cfp1^{fl/fl}Cd21^{Cre}$ mice relative to the controls, whereas cells in S or G2/M phases were decreased (Fig. 1I). Consistently, the proliferation index obtained from CFSE staining of activated $Cfp1^{fl/fl}Cd21^{Cre}$ cells was reduced compared to controls (Fig. 1J). Taken together, we conclude that CFP1 is required for B cell activation and cell cycle progression during the germinal center response.

Cfp1 deletion after B cell activation impairs germinal center response

To overcome the defective activation of $Cfp1^{fl/fl}Cd21^{Cre}$ B cells and dissect the effect of *Cfp1* on GCB cells following their activation, we conditionally deleted *Cfp1* in activated B cells by breeding $Cfp1^{fl/fl}$ mice with the $Aicda^{Cre}$ line[30]. *Cfp1* was efficiently deleted in the GCB cells by the $Aicda^{Cre}$ (Fig. S2D–F). In contrast to $Cfp1^{fl/fl}Cd21^{Cre}$ mice, the frequency of $B220^+IgD^-CD138^-CD38^+GL7^+$ activated precursors in $Cfp1^{fl/fl}Aicda^{Cre}$ mice immunized with NP-KLH/Alum was indistinguishable from $Cfp1^{fl/fl}$ littermates at 3 days p.i. and onwards (Fig. S3A). The frequencies and numbers of GC B cells in the form of $B220^+IgD^-CD138^-CD38^-GL7^+$ (Fig. S3B) or $B220^+CD95^+GL7^+$ (Figs. 2A and S3C) in $Cfp1^{fl/fl}Aicda^{Cre}$ mice were significantly reduced relative to controls during the course of immunization. Administration with NP-KLH/MnJ reproduced an over threefold reduction in splenic GCB cells at day 14 p.i. in *Cfp1* deficient mice (Fig. 2B and S3D). To further demonstrate GC entry of $Cfp1^{fl/fl}Aicda^{Cre}$ cells, we stained immunized splenic cells with additional sets of established surface markers including PNA and EFNB1[31]. *Cfp1* deletion markedly reduced the florescence intensity of CD95, PNA and EFNB1 (Fig. S4A) and the fraction of GCB cells identified by the combination of CD95 with PNA or EFNB1 (Fig. S4B). Although markedly reduced (~fourfold versus controls) upon *Cfp1* loss, $B220^+IgD^-CD95^+CD38^-GL7^+PNA^+EFNB1^+$ GCB cells were still identifiable in ~1% of splenic B cells, confirming impaired but genuine GC entry (Fig. 2C). In addition, $IgG1^+$ and NP^+ GCB cells were diminished in $Cfp1^{fl/fl}Aicda^{Cre}$ mice (Fig. 2D). In line with severely impaired antibody response, ELISA analysis of sera from *Cfp1* deficient mice at day 14 p.i. showed lower titers of NP-specific IgG1 antibodies for low-affinity NP_{32} or high-affinity NP_2 (Fig. 2E). A significantly lower NP_2/NP_{32} EC50 ratio in $Cfp1^{fl/fl}Aicda^{Cre}$ mice indicated defective antibody affinity maturation (Fig. 2F).

https://doi.org/10.1038/s41467-025-63291-8

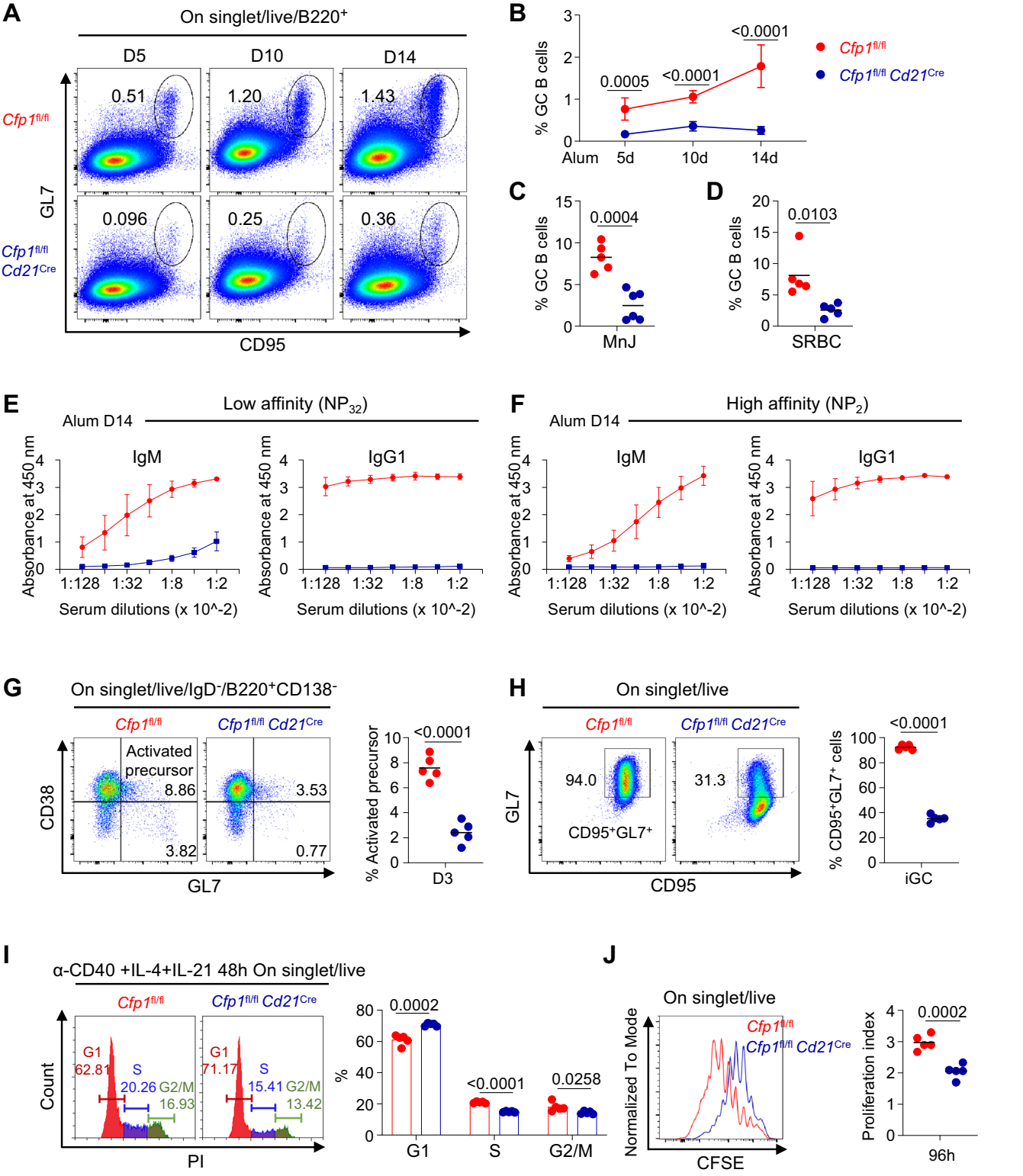

To further address defective antibody affinity maturation upon *Cfp1* loss, we analyzed the mutation profiles of the J_H4 region in *Cfp1*$^{fl/fl}$*Aicda*^{Cre} and control GCB cells by a high-throughput method, SHM-seq[32]. Mutations in control cells were enriched at WRC motifs with frequencies as high as 6×10^{-3}/nt/generation were observed. *Cfp1* ablation led to an 8.4-fold reduction in the overall mutation frequency (Fig. 2G). SHM occurs in the fast-dividing DZ B cells. GC zoning analysis indicated that the ratio of DZ B cells was significantly decreased from ~65% in control mice to only 30% in *Cfp1*-deficient mice with a concomitant increase of LZ cells from 30% to over 60% (Fig. 2H). Thus, *Cfp1* deletion led to diminished DZ B fraction and somatic hypermutations.

The reversed DZ/LZ ratio in *Cfp1*$^{fl/fl}$*Aicda*^{Cre} mice may result from impaired GCB cell proliferation and/or increased apoptosis. FACS analysis indicated that apoptosis by active caspase3 staining in the total GCB or DZ/LZ B cells was not significantly changed upon *Cfp1* deletion (Fig. 2I). Examining the proliferation of GCB cells via Ki67 staining, we found a clear reduction of Ki67$^+$ GCB cells from *Cfp1*$^{fl/}$

Fig. 1 | *Cfp1* loss impairs B cell activation and germinal center entry. A, **B** Flow cytometry plots and ratio of splenic GCB ($B220^+CD95^+GL7^+$) cells at different time post immunization with NP-KLH/Alum. Data were pooled from three independent experiments; $Cfp1^{fl/fl}$ (Day5/10/14 $n = 5$; 3 males (m), 2 females (f)); $Cfp1^{fl/fl}$ $Cd21^{Cre}$ (Day5/10/14 $n = 6$; 3 m, 3 f). $p < 0.0001$ (10d = 7.68e−6, 14d = 4.50e−5). **C** The percentage of splenic GCB cells of $Cfp1^{fl/fl}$ and $Cfp1^{fl/fl}$ $Cd21^{Cre}$ mice on day 14 p.i. with NP-KLH/MnJ. Data were from two independent experiments; $Cfp1^{fl/fl}$ ($n = 5$; 3 m, 2 f); $Cfp1^{fl/fl}$ $Cd21^{Cre}$ ($n = 6$; 3 m, 3 f). **D** The percentage of splenic GCB cells of $Cfp1^{fl/fl}$ and $Cfp1^{fl/fl}$ $Cd21^{Cre}$ mice on day 12 p.i. with SRBC. Data were from two independent experiments; $n = 5$; 3 m, 2 f. **E**, **F** ELISA for serum NP-specific low-affinity (NP_{32}) and high-affinity (NP_2) IgM and IgG1 antibodies from $Cfp1^{fl/fl}$ and $Cfp1^{fl/fl}$ $Cd21^{Cre}$ mice on day 14 p.i. with NP-KLH/Alum; $n = 5$; 3 m, 2 f. **G** Representative flow plots and ratio of activated precursors ($IgD^-B220^+CD138^-GL7^+CD38^+$) in the spleen of NP-KLH/Alum-immunized $Cfp1^{fl/fl}$ and $Cfp1^{fl/fl}$ $Cd21^{Cre}$ mice analyzed on day 3. Data were pooled from two independent experiments; $n = 5$; 3 m, 2 f. $p < 0.0001$ (= 2.01e−5). **H** Representative flow plots and ratio of day 4 iGC B cells from $Cfp1^{fl/fl}$ and $Cfp1^{fl/fl}$ $Cd21^{Cre}$ mice cultured on 40LB with the presence of IL-4. $n = 5$; 1 m, 4 f. $p < 0.0001$ (= 3.11e−10). **I** Cell cycle analysis of anti-CD40/IL-4/IL-21 stimulated splenic $Cfp1^{fl/fl}$ and $Cfp1^{fl/fl}$ $Cd21^{Cre}$ B cells for 4d (red: G1; blue: S; green: G2/M). Data were pooled from two independent experiments; $n = 5$; 1 m, 4 f. $p < 0.0001$ (= 6.10e−8). **J** Representative histogram (red: $Cfp1^{fl/fl}$; blue: $Cfp1^{fl/fl}$ $Cd21^{Cre}$) and quantification of CellTrace CFSE staining for cells in (**I**). Data were pooled from two independent experiments; $n = 5$; 1 m, 4 f. **B**, **E**, **F** Data points represent the mean ± SD. **C**, **D**, **G**, **H**, **I**, **J** Each symbol indicates one mouse and lines denote means. **I** Bars represent the mean. *P*-values by unpaired *t*-test (two-tailed).

$^{fl}Aicda^{Cre}$ mice compared to controls (Fig. 2J). Cell cycle analysis indicated a significantly increased segment of G1-phase cells and reduced cells into S-phase in $Cfp1^{fl/fl}Aicda^{Cre}$ mice (Fig. 2K). Collectively, these data demonstrated that *Cfp1* deletion caused significant defects in the S phase-entry and proliferation of GCB cells that could in turn contributes to severely diminished somatic hypermutation and affinity maturation.

Cfp1 ablation impacts H3K4me3 on genes linked to GC B cell functions

We next set to investigate whether histone modification by *Cfp1* is involved in B cell response. To this end, we conducted CUT&Tag assay to analyze the global H3K4me3 profiles in GCB cells from $Cfp1^{fl/fl}Aicda^{Cre}$ and control mice. A total of 11,358 H3K4me3 peaks were identified from control GCB cells and the vast majority of these peaks were retained upon *Cfp1* loss (Fig. S5A). As expected, over 85% of H3K4me3 peaks were situated at promoter-proximal regions in both control and $Cfp1^{fl/fl}Aicda^{Cre}$ GCB cells (Fig. S5B). Surprisingly, the overall H3K4me3 signal strengths in $Cfp1^{fl/fl}Aicda^{Cre}$ GCB cells around the transcription start site (TSS) were slightly elevated, as only 525 peaks experienced reduction and 3340 peaks showed significant signal gain in $Cfp1^{fl/fl}Aicda^{Cre}$ GCB cells (Fig. S5C, D and Supplementary data 1). Examination of those altered peaks revealed that they have similar signal strength in control cells, and the ones with reduced H3K4me3 signals in the *Cfp1*-KO cells tended to be wider in breadth (Fig. S5E, F). Gene ontology (GO) analysis for peaks with differential H3K4me3 signals indicated that H3K4me3 peaks with significant signal loss upon *Cfp1* deletion were enriched in genes of cell activation (*Cd19, Pou2af1, Mef2b, Spi1, Aicda*, etc.) and mitotic cell cycle (*Mybl1, Tubb5, Birc5, Cdc6*, etc.), closely linked to GCB functions (Fig. S5G, H). Conversely, genes with increased H3K4me3 peaks were enriched in cell projection organization (*Cd38, Klf4, Efna1, Efna5, Efnb2*, etc.) and morphogenesis (*Prdm1, Bcl2, S1pr1, Hhex, Bhlhe40*, etc.), many of which have been shown to be involved in memory B cell differentiation (see below) (Fig. S5G, H). Therefore, *Cfp1* is responsible for H3K4me3 modifications at a small subset of genes that were enriched in pathways crucial to the identity and/or functions of GCB cells without affecting overall H3K4me3 distribution patterns.

Association of CFP1 and H3K4me3 peaks with CpG islands

Prior studies have revealed preferential CFP1 association to unmethylated CpG islands (CGI)[20]. To assess the CGI dependence of CFP1 binding and H3K4me3 modification in GCB cells, we profiled CFP1 genome association by chromatin immunoprecipitation (ChIP). Out of 5087 CFP1-bound peaks, ~50% (2523/5087) colocalized with CpG sites, such as *Gpr19* and non-CpG gene *Smim3* (Fig. S6A–C). In contrast, only 15.4% (2523/16,339) of CGI sites were bound by CFP1 (Fig. S6A). This ratio is significantly lower than the reported 81% bound rate of CGIs by CFP1 in the brain[20] and close to the 6% bound rate in mature T cells[24], highlighting cell type specific CFP1 association to CGIs. 78% (8867/11,358) of H3K4me3 peaks were located at the CpG sites and predominantly associated with promoters (Fig. S6A, B). The average H3K4me3 signal at the CpG group is higher compared to the non-CpG group. Notably, *Cfp1*-deletion led to an increase in H3K4me3 signals at both CpG and non-CpG sites (Fig. S6D). Lastly, while 85.8% of H3K4me3 signal gain was associated with CpG sites, the peaks with signal loss upon *Cfp1* deletion were evenly seen at CpG and non-CpG sites (Fig. S6E, F). Taken together, we conclude that a significant fraction of CFP1 and H3K4me3 peaks were associated with CGIs, and CFP1 could modulate this histone mark through mechanisms not strictly dependent on CpG status in GCB cells.

H3K4me3 redistributes from active to bivalent promoters upon *Cfp1* loss

To elucidate chromatin features underlying differential H3K4me3 changes upon *Cfp1* loss, we profiled the genomic distribution of H3K4me3, H3K27me3, CFP1 and RNA Pol II in control mice with ChIP-seq (for CFP1) and CUT&Tag (for H3K27me3 and Pol II). Chromatin states were systematically classified by ChromHMM[33,34], yielding a six-state model that distinguished bivalent, repressed, null (no mark), permissive and active chromatin states based on distinct factor/modification features (Fig. S7A). As anticipated, H3K4me3 exhibited strong association with active chromatin states and modest enrichment at bivalent states, with the former primarily localizing to CpG islands, TSS proximity and exons (Fig. S7B). Notably, 81% (7876/9711) of total H3K4me3-bound genes harbored active promoters (Of these, 93.9% (7397/7876) exhibited concurrent gene expression and were further designated as active), and only 19% were bivalent (Fig. S7C, upper, Supplementary data 2), consistent with previous reports[35]. *Cfp1* preferentially binds to active (66%, 2544/3856) over bivalent genes (12.5%, 482/3856) (Fig. S7C, lower). In addition, the H3K4me3 signal at active genes was stronger than bivalent promoters (Fig. S7D). Intriguingly, promoters gaining H3K4me3 upon *Cfp1* loss exhibited significantly higher baseline H3K27me3 in controls compared to those losing H3K4me3 (Fig. S7E, F). Moreover, 75.2% of promoters with H3K4me3 loss mapped to active genes, while a third of H3K4me3-gaining promoters were bivalent or repressed (Fig. S7G). This data collectively suggests a redistribution model where *Cfp1* maintains H3K4me3 at active genes while restricting its deposition at poised/repressed regions.

Cfp1 does not affect H3K4me3 broad domains in GC-B cells

Recent studies have demonstrated that Setd1A/B play a crucial role in establishing broad H3K4me3 peaks associated with cell-identity gene transcription in mES cells or spermatogonia[36,37]. Given the relative broader width of peaks with H3K4me3 signal loss upon *Cfp1* deletion, we asked whether CFP1 regulates H3K4me3 broad peaks in GCB cells. We define the top 5% widest H3K4me3 peaks as broad domains[38] with a cutoff breadth of 5.5 kb (Fig. S8A). Genes linked to these broad peaks were enriched in lymphocyte activation and regulation of cell differentiation (Fig. S8B). However, unlike in mES cells or spermatogonia, *Cfp1* deletion in GCB cells did not significantly alter the number, ratio,

https://doi.org/10.1038/s41467-025-63291-8

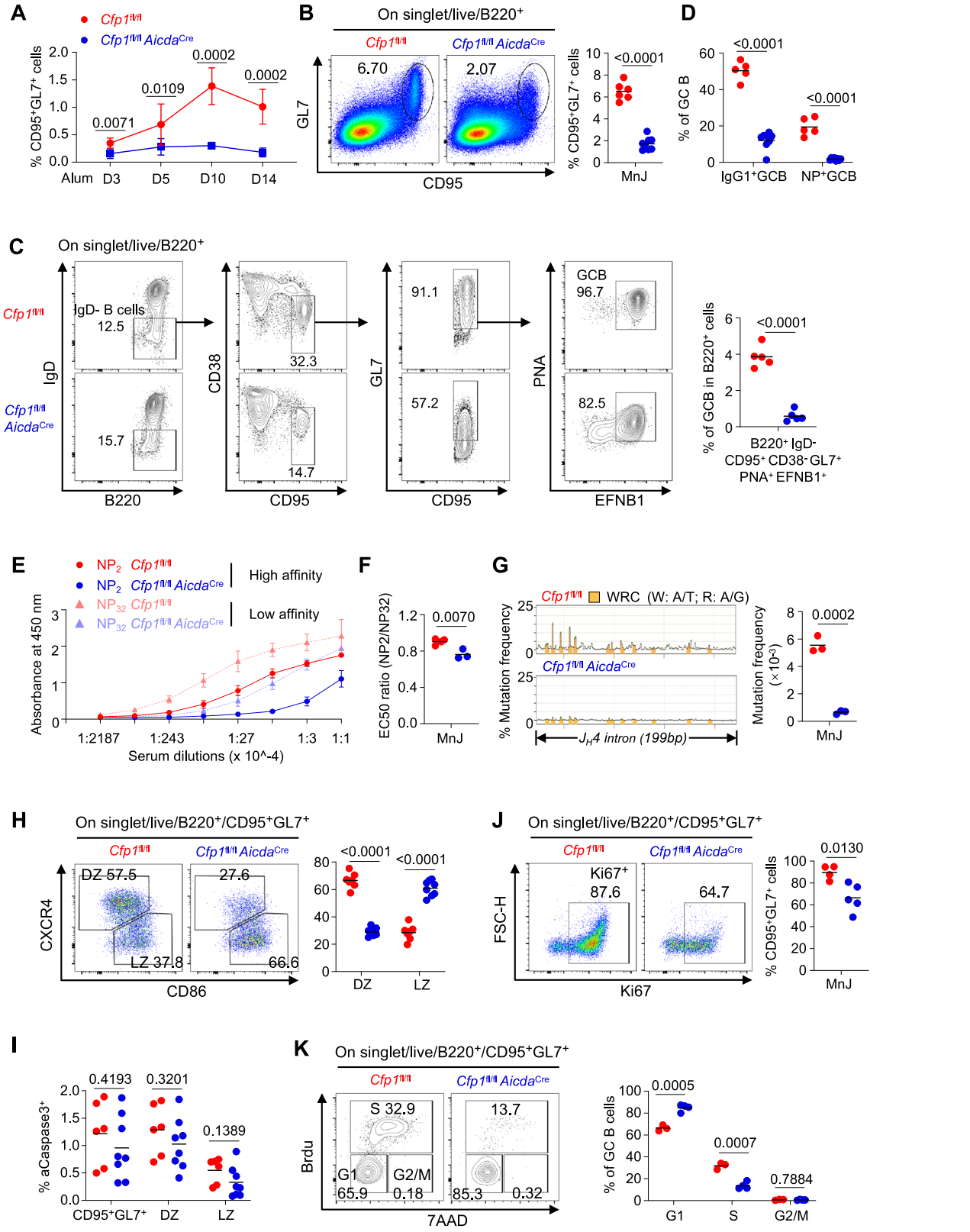

average width or intensity of H3K4me3 broad domains (Fig. S8C, D), suggesting that GCB cells employ redundant HMTs beyond Setd1A/B or distinct mechanisms to establish/maintain these domains. Furthermore, since broad H3K4me3 domains are associated reduced RNA Pol II pausing[21] (Fig. S8E, F), we examined whether CFP1 influences Pol II recruitment. Global Pol II binding and pausing at H3K4me3 broad or random peaks remained largely unchanged by *Cfp1* loss (Fig. S8G, H), reinforcing that *Cfp1* is dispensable for transcription-associated H3K4me3 broad domains in GCB cells.

Cfp1 regulates transcription of a subset of GCB genes

Promoter-bound H3K4me3 has been shown to be associated with active transcription[16]. To investigate whether the change in H3K4me3 marks upon *Cfp1* deletion in GC B cells affects gene transcription, we

Fig. 2 | *Cfp1* deletion after B cell activation impaired germinal center responses. **A** The percentage of splenic GCB cells in *Cfp1*$^{fl/fl}$ and *Cfp1*$^{fl/fl}$ *Aicda*^{Cre} mice immunized with NP-KLH/Alum at different time points. Data were from three independent experiments; *Cfp1*$^{fl/fl}$ (Day3/5 $n = 6$; 3 males (m), 3 females (f); Day 10/14 $n = 6$; 3 m, 3 f); *Cfp1*$^{fl/fl}$ *Aicda*^{Cre} (Day3 $n = 5$; 2 m, 3 f; Day5 $n = 9$; 5 m, 4 f; Day10 $n = 5$; 2 m, 3 f; Day14 $n = 6$; 3 m, 3 f). **B**–**K** Mice were immunized with NP-KLH/MnJ, boosted on day 8 and analyzed on day 14. **B** Flow cytometry plots and ratio of splenic GCB cells from *Cfp1*$^{fl/fl}$ and *Cfp1*$^{fl/fl}$*Aicda*^{Cre} mice. Data were from three independent experiments; *Cfp1*$^{fl/fl}$ ($n = 6$; 3 m, 3 f); *Cfp1*$^{fl/fl}$ *Aicda*^{Cre} ($n = 8$; 4 m, 4 f). $p < 0.0001$ (= 2.20e−8). **C** Flow cytometry plots and ratio of splenic GCB cells (B220^{+}IgD^{-}CD95^{+}CD38^{-}GL7^{+}EFNB1^{+}PNA^{+}) from *Cfp1*$^{fl/fl}$ and *Cfp1*$^{fl/fl}$*Aicda*^{Cre} mice. Data were from two independent experiments; $n = 5$; 3 m, 2 f. $p < 0.0001$ (= 4.19e−6). **D** The percentage of splenic IgG1^{+} and antigen-specific (NP^{+}) GCB cells. Data were pooled from three independent experiments. *Cfp1*$^{fl/fl}$ ($n = 5$; 3 m, 2 f); *Cfp1*$^{fl/fl}$ *Aicda*^{Cre} ($n = 8$; 4 m, 4 f). p<0.0001 (IgG1^{+} = 3.32e−8, NP^{+} = 4.90e−7). **E** ELISA for serum NP_{32} and NP_2 IgG1 antibodies from *Cfp1*$^{fl/fl}$ and *Cfp1*$^{fl/fl}$ *Aicda*^{Cre} mice on day 14 p.i. **F** EC_{50} for NP_2 relative to NP_{32} from two independent experiments; *Cfp1*$^{fl/fl}$ ($n = 4$; 2 m, 2 f); *Cfp1*$^{fl/fl}$ *Aicda*^{Cre} ($n = 3$; 2 m, 1 f). **G** Mutation profile of the J_H4 region in GCB cells from control and *Cfp1*$^{fl/fl}$*Aicda*^{Cre} mice. $n = 3$; 2 m, 1 f. The *y* axis indicates mutation frequency calculated as percentage of sequences containing a mutation at each nucleotide over total sequenced reads. The overall mutation frequency in the entire J_H4 region in control and *Cfp1*$^{fl/fl}$*Aicda*^{Cre} mice was shown (right). **H** Flow cytometry plots and ratio of DZ and LZ GCB cells. *Cfp1*$^{fl/fl}$ ($n = 7$; 3 m, 4 f); *Cfp1*$^{fl/fl}$ *Aicda*^{Cre} ($n = 8$; 4 m, 4 f). $p < 0.0001$ (DZ = 4.59e−10, LZ = 5.65e−8). **I** Apoptosis of GCB cells by active Caspase3 staining. *Cfp1*$^{fl/fl}$ ($n = 6$; 3 m, 3 f); *Cfp1*$^{fl/fl}$ *Aicda*^{Cre} ($n = 8$; 4 m, 4 f). **J** GCB cell proliferation analysis by Ki67 staining. Data were pooled from two independent experiments. *Cfp1*$^{fl/fl}$ ($n = 4$; 2 m, 2 f); *Cfp1*$^{fl/fl}$ *Aicda*^{Cre} ($n = 5$; 2 m, 3 f). **K** Cell cycle analysis of GC B cells by BrdU incorporation and 7-AAD staining. Data were from two independent experiments; *Cfp1*$^{fl/fl}$ ($n = 3$; 2 m, 1 f); *Cfp1*$^{fl/fl}$ *Aicda*^{Cre} ($n = 4$; 2 m, 2 f). **A**, **E** Data points represent the mean ± SD. *P*-values by unpaired *t*-test (two-tailed).

assayed mRNA transcripts in control and *Cfp1*$^{fl/fl}$ *Aicda*^{Cre} GCB cells by bulk RNA-sequencing. A total of 3101 differentially expressed genes with 1591 upregulated and 1510 downregulated (p-value < 0.05, absolute $\log_2$ FC > 0.5) were identified in *Cfp1*-deficient GC B cells (Fig. 3A). GO analysis revealed that the downregulated genes in *Cfp1*$^{fl/fl}$*Aicda*^{cre} GC B cells were enriched in pathways including mitotic cell cycle/DNA replication/DNA metabolism and the immunoglobulin-mediated immune response, etc. Conversely, the upregulated genes were enriched in innate immune response, cell adhesion, inflammatory responses, etc. (Fig. 3B). The downregulation of DNA replication genes was in accordance with defective in S phase entry observed in *Cfp1*-deficient GCB cells (Fig. 2K).

We then explored whether the change of transcription in *Cfp1*-KO GCB cells can be attributed to alterations in H3K4me3 at these genes. Genes with H3K4me3 loss upon *Cfp1* deletion appeared to have significantly higher expression in control cells compared to those with no change or gain in this modification. Conversely, genes with increased H3K4me3 mark at the promoter exhibited rather low expression in control cells (Fig. 3C). A positive correlation between transcriptional change and H3K4me3 alteration was observed (Fig. 3D). In addition, genes showing reduction in both mRNA expression and H3K4me3 signal (the both down group) upon *Cfp1* deletion tended to have significantly wider H3K4me3 peaks in controls, while those with increased mRNA and H3K4me3 modification (both up) bore narrower H3K4me3 peaks (Fig. 3E, F). GO analysis suggested that both down genes were enriched in cell cycle and GC formation, etc. and the both up genes were enriched in pathways of cell adhesion/migration and signaling to growth factor stimulus (Fig. 3G). For instance, the *Cdc6* gene vital for the initiation of DNA replication[39], and the *Aicda* gene that is essential for both SHM and CSR[40], were downregulated with diminished promoter H3K4me3 in *Cfp1*-deficient cells (Fig. 3H; Fig. S13 and Supplementary Table 3). *Aicda* downregulation may contribute to the impaired affinity maturation and IgG1 CSR (Fig. 2D–G). The sphingosine-1-phosphate receptor 1 (*S1pr1*) gene regulating B cell egress from the follicles[41] was significantly upregulated with elevated H3K4me3 at the promoter (Fig. 3H).

Cfp1 suppresses inflammatory programs in GCB cells

A recent study demonstrated the critical role of inflammatory signaling in impeding GC response that is regulated by the *Arid1a*-containing chromatin remodeling complex BAF[42]. Gene Set Enrichment Analysis (GSEA)[43] with mouse ontology gene sets (https://www.gsea-msigdb.org/gsea/msigdb/index.jsp) indicated that genes involved in the regulation of innate immune response and regulation of inflammatory response were significantly upregulated in *Cfp1*$^{fl/fl}$*Aicda*^{Cre} GC B cells (Fig. S9A). Inflammatory genes under negative control by *Arid1a* or suppressed by *Cfp1* exhibited 20% overlap (Fig. S9B). Importantly, genes involved in innate immune response, cytokine signaling, inflammatory response, and chemotaxis that were significantly upregulated in the absence of *Cfp1*, for instance, *Ccr12* and *Tlr3*, harbored markedly increased H3K4me3 signal intensity at the promoter-proximal regions (Fig. S9C–E). *Arid1a* itself is not affected by *Cfp1* deficiency (Fig. S9F), indicating separate regulation of the inflammatory genes by the chromatin remodeling and modification complexes. These data collectively suggest that *Cfp1* suppresses the expression of inflammatory genes that discourage GC responses through modulating H3K4me3 modifications.

Cfp1 is critical for maintaining *Bcl6* expression in GC B cells

Bcl6 is a key transcriptional suppressor for GCB fate determination and differentiation[9,44]. Approximately fourfold decreases in *Bcl6* mRNA and protein levels in *Cfp1*-depleted GCB cells were observed by RNA-seq and intracellular staining (Fig. 4A, B). Compared to controls, the BCL6^{+} population within CD95^{+}GL7^{+} GCB cells was significantly reduced by more than twofold in *Cfp1*$^{fl/fl}$*Aicda*^{cre} mice immunized with NP-KLH/MnJ (Fig. 4C) or NP-KLH/alum from day 3 p.i. onwards (Fig. 4D), confirming the failure of *Cfp1*-depleted B cells to commit a GCB fate. *Bcl6* suppresses a spectrum of downstream target genes in GCB cells. GSEA analysis with a *Bcl6* target gene set from earlier studies[45,46] indicated increased transcription of majority of these genes, for instance *Cd69*[45], in *Cfp1*$^{fl/fl}$*Aicda*^{Cre} GCB cells, consistent with the positive regulation of *Bcl6* by *Cfp1* (Fig. 4E, F). Surprisingly, only mild reduction in H3K4me3 at the *Bcl6* promoter, despite Cfp1 binding at nearby CpG sites, was observed in *Cfp1*-deleted cells (Fig. 4A), implicating additional mechanisms beyond direct binding to regulate *Bcl6* expression by *Cfp1*.

The transcriptional regulation of *Bcl6* involves various factors, including transcription factors, epigenetic regulators and three-dimensional genome folding that loops the *Bcl6* enhancers to the promoter. Previous studies have identified transcription factors MEF2B and OCTs[8,9,47–50] that form a ternary complex with OCA-B to activate *Bcl6* expression by bolstering E-P looping[48]. Interestingly, the expression of *Mef2b* and *Pou2af1* (gene encoding OCA-B) were both reduced accompanied by marked reduction in H3K4me3 in *Cfp1*$^{fl/fl}$*Aicda*^{Cre} GCB cells (Fig. 4G). To further study the mechanism of CFP1 in *Bcl6* regulation, we performed chromosome conformation capture coupled-sequencing (4C-HTGTS) with an anchor primer at the *Bcl6* promoter (Fig. 4H). The results indicated that interactions between the *Bcl6* promoter and enhancer clusters #1 or #2 critical for E-P looping and *Bcl6* induction[48], were both substantially diminished in *Cfp1*-depleted GCB cells (Fig. 4H, I). The reduced E-P looping was confirmed by the 3C assay (Fig. 4J). These findings suggest that likely through H3K4me3 modification, *Cfp1* positively regulates the expression of early GC factors *Mef2b* and *Pou2af1* which in turn

https://doi.org/10.1038/s41467-025-63291-8

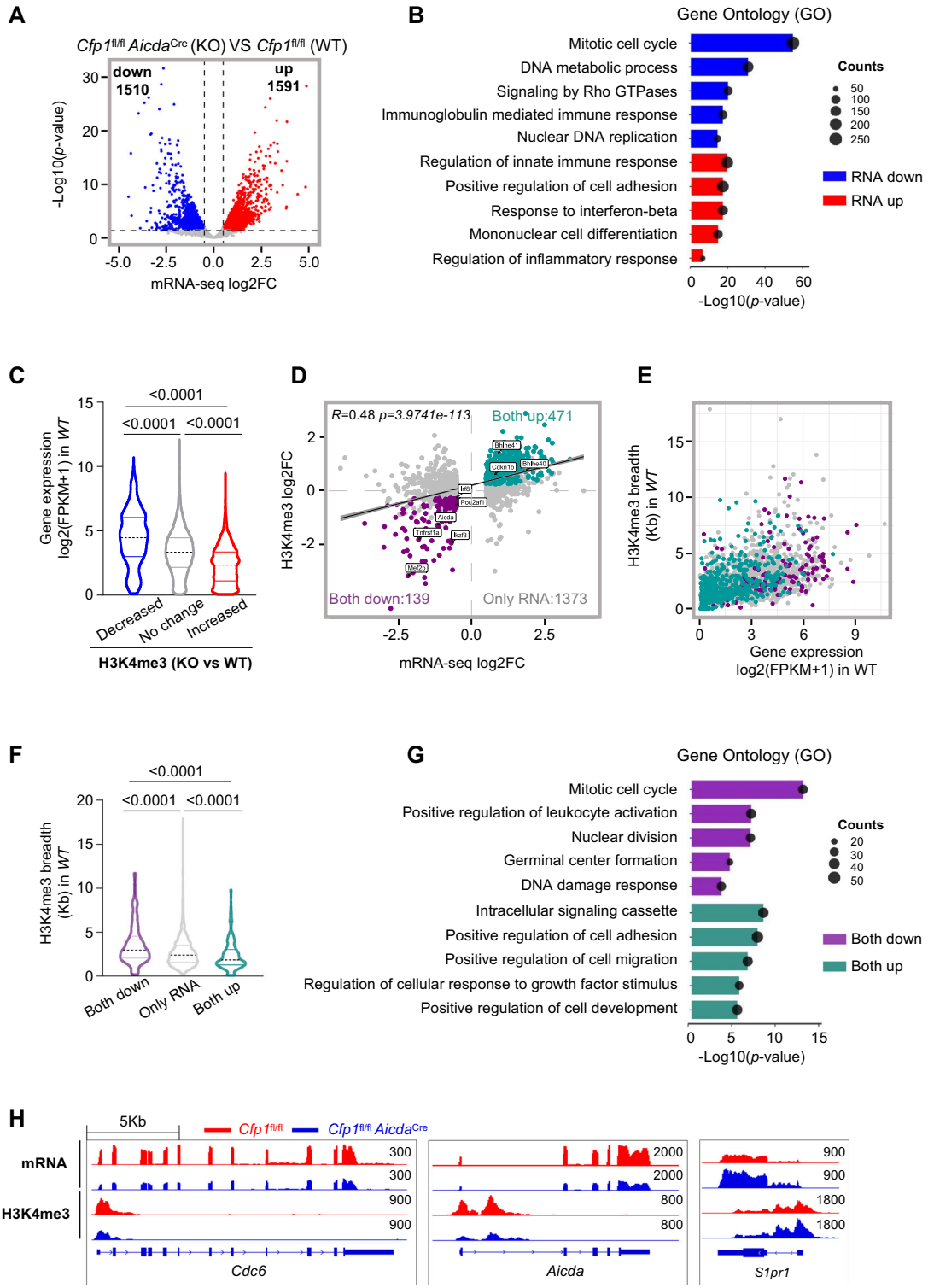

facilitate *Bcl6* E-P looping and transcription activation for GCB fate determination.

In addition, a recent study revealed that the IL-4-STAT6 axis activates *Bcl6* expression by recruiting histone demethylase UTX to the enhancers to demethylate H3K27me3[51]. We found that H3K27me3 levels at downstream enhancer 2 were markedly increased accompanied with decreased H3K4me3 and reduced eRNA in *Cfp1*-deficient cells compared to controls (Fig. 4H). Therefore, controlling the enhancer activity through modulating H3K4me3 and H3K27me3 levels at the enhancer could serve as another functional mechanism for *Cfp1* in *Bcl6* expression regulation.

Cfp1-deficient GCB cells have greater propensity to differentiate into plasma cells

Irf4 is a *Bcl6* target that is required for plasma cell differentiation[11,52]. In line with markedly reduced *Bcl6* expression in *Cfp1*-deficient GCB cells, significantly augmented IRF4 expression by intracellular staining and mRNA-seq was observed (Fig. 5A, B). The level of H3K4me3 at the *Irf4* promoter in *Cfp1*-KO cells was indistinguishable from controls, despite evident CFP1 binding in the gene body, suggesting that increased *Irf4* expression upon *Cfp1* loss may result indirectly from reduced *Bcl6*, or alternatively, *Cfp1* might regulate *Irf4* expression through mechanisms independent of histone modification. Interestingly, an over twofold

Fig. 3 | *Cfp1* regulates H3K4me3 modification for proper GCB gene transcription. Mice were immunized with NP-KLH/MnJ, boosted on day 8 and GCB cells were sorted on day 14 for bulk mRNA-seq and CUT&Tag; $n = 3$; 3 females (f). **A** Volcano plot for differentially expressed genes from *Cfp1*$^{fl/fl}$*Aicda*^{Cre} (KO) versus *Cfp1*$^{fl/fl}$ (WT) GC B cells (Fold change >1.4-fold; *p*-values < 0.05; blue: down; red: up). **B** GO enrichment of differentially expressed genes. Top 5 enriched pathways ranked by *q*-values for upregulated and downregulated genes are shown (blue: down; red: up). **C** Violin plot showing the distribution and average RNA expression levels in control GCB cells for genes with increased (red), decreased (blue), or unchanged H3K4me3 (grey) at promoters upon *Cfp1* loss. **D** Scatter plot for the correlation between changes in gene expression (DEGs from **A**) and altered H3K4me3 at promoters from *Cfp1*-KO versus control GCB cells (green: both up; purple: both down; grey: only RNA). Pearson correlation coefficient was shown. The black line shows the best-fit linear relationshipbetween the *x*-axis and *y*-axis values, and grayish shadow around the black line represents the 95% confidence interval of the model. **E** Scatter plot for the distributions of H3K4me3 peak breadth and expression RNA in control GCB cells for both up, both down, and only RNA genes identified in (**D**). **F** Violin plot showing the average H3K4me3 peak width in each category. **G** The top five pathways ranked by *q*-values for the both down and both up categories of genes identified in (**D**). **H** Genome browser track of example both down and both up genes related to GC B cell functions (red: *Cfp1*$^{fl/fl}$; blue: *Cfp1*$^{fl/fl}$ *Aicda*^{Cre}). **C**, **F** The black lines show the medians, with the upper and lower quartiles above and below them. *P*-values was calculated by unpaired Wilcoxon rank sum test (two-tailed).

increase in the ratio of CD138$^+$ in CD95$^+$GL7$^+$ GCB cells from *Cfp1*$^{fl/fl}$*Aicda*^{Cre} mice compared to controls was observed (Fig. 5C). Accordingly, the frequency of plasma cells in splenic B cells from *Cfp1*$^{fl/fl}$*Aicda*^{Cre} mice was only mildly reduced despite severe defect in GC induction (Fig. 5D). These data suggest that *Cfp1*-deficient germinal center B cells exhibit an increased propensity to differentiate into plasma cells, presumably due to elevated IRF4 expression.

PCs can be generated through the extrafollicular and the GC pathways[53,54]. To examine whether *Cfp1* impacts PC formation by the extrafollicular pathway, we immunized *Cfp1*$^{fl/fl}$, *Cfp1*$^{fl/fl}$*Cd21*^{Cre} or *Cfp1*$^{fl/fl}$*Aicda*^{Cre} mice with NP-KLH/Alum and examined B220$^+$IgD$^-$CD138$^+$ PC at day 3 or day 5 p.i. (Fig. S10A, B) when PC formation occurs exclusively through the extrafollicular pathway. The decline in the ratio and number of PCs in control animals at day 5 compared to day 3 p.i. was observed, consistent with the transient nature of extrafollicular response (Fig. S10C). Notably, *Cfp1* deletion by either Cre did not change the ratio and absolute counts of PCs (Fig. S10C), indicating that *Cfp1* is dispensable for early PC formation via the extrafollicular pathway.

PC precursors (pre-PC) have been identified by a recent study as BCL6^{lo}IRF4$^+$CD69$^+$ cells in the LZ compartment of the GC[55,56]. A 3~4-fold increase in BCL6^{lo}IRF4$^+$CD69$^+$ pre-PC within LZ B cells from *Cfp1*-deficient mice compared to controls was observed (Figs. 5E; S10D), further confirming that *Cfp1*-deficient GC B cells have greater propensity to differentiate towards PC progenitors.

To directly investigate whether *Cfp1* regulates PC differentiation in a cell-autonomous manner, we performed Nojima culture of *Cfp1*$^{fl/fl}$, *Cfp1*$^{fl/fl}$*Cd21*^{Cre} B cells on 40LB feeder cells supplemented with IL-4 followed by IL-21 to facilitate plasma cell formation (Fig. 5F). Under this condition, 5.8% of control B cells were CD138$^+$, whereas this faction rose to 14.4% in *Cfp1*-deficient cells (Fig. 5G) that also exhibited significantly elevated IRF4 signal intensity (Fig. 5H). Aligning with our in vivo observation of augmented potential of PC formation in *Cfp1*-deficient GCB cells, this data revealed the cell-intrinsic role of *Cfp1* in regulating GC-to-PC transition.

Cfp1 restrains memory B cell differentiation by suppressing pre-MBC genes

We next examined whether memory B cell formation was influenced by *Cfp1* through analyzing antigen-specific B cells. Interestingly, from day 5 p.i. with NP-KLH/alum onwards, significantly higher ratio of B220$^+$NP$^+$IgD$^-$CD138$^-$CD38$^+$GL7$^-$ memory B cells (Fig. S11 A for gating strategy) was observed in *Cfp1*$^{fl/fl}$*Aicda*^{Cre} mice (Fig. 6A, B). The total number of NP$^+$ MBCs was indistinguishable at day 5 and 10 p.i. and reduced by 2.33-fold at day 14 in *Cfp1*-KO mice compared to controls (Fig. 6B). Due to severe defect in the expansion of NP$^+$ cells (Fig. 6C), the ratio of NP$^+$ MBC in total NP$^+$ cells was significantly elevated in the day 10 and day 14 (Fig. 6D). Immunization with NP-KLH/MnJ for 14 days reproduced the phenotype of MBC accumulation in *Cfp1*-KO mice (Fig. 6E–H). Memory B cells can be generated both extrafollicularly and intrafollicularly[9,12,28,31,57,58]. To assess the relative contributions of these two pathways to memory B cell accumulation, we examined the extent of GC-derived (CD80$^+$PD-L2$^+$) and non-GC-derived (CD80$^-$PD-L2$^-$) memory B cells[59]. *Cfp1*-ablation did not change the relative odds of GC versus non-GC-derived MBCs (Fig. 6 I). Taking into account the greater probability of MBC cell differentiation upon *Cfp1* loss, both GC-and non-GC-derived NP$^+$ MBCs were markedly increased by 2~3-fold in *Cfp1*$^{fl/fl}$*Aicda*^{Cre} mice (Fig. 6J). Moreover, we also examined NP$^+$IgG1$^+$ MBC cells. Although the ratio of NP$^+$IgG1$^+$ cells was drastically reduced upon *Cfp1* loss, suggestive of severely impaired IgG1 class switching (Fig. 6K), NP$^+$IgG1$^+$CD38$^+$GL7$^-$ MBC (Fig. S11B for gating strategy) ratio was still expanded by fourfold in *Cfp1*$^{fl/fl}$*Aicda*^{Cre} mice compared to controls (Fig. 6L). We therefore concluded that *Cfp1* restrains the differentiation of both extrafollicular and intrafollicular memory B cells.

Recent studies have identified subsets of memory B precursors (pre-MBC) that are GCB cells in the transition to become MBCs[31,57,58,60]. Different panels of surface proteins were used to identify pre-MBCs. In this regard, CCR6$^+$CD38$^+$ cells in the CD95$^+$GL7$^+$ population were reported as functional MBC precursors[57]. Examining the B220$^+$IgD$^-$CD95$^+$GL7$^+$CCR6$^+$CD38$^+$ (Fig. S11C for gating strategy) cells upon NP-KLH/MnJ immunization, we found an over sixfold increase of this population in *Cfp1*$^{fl/fl}$*Aicda*^{Cre} mice compared to controls (Fig. 7A), indicating that *Cfp1* deletion favors differentiation of GCB towards MBC. CCR6$^+$CD38$^+$ pre-MBCs exhibited significantly reduced proliferative activity indicated by less EdU incorporation compared to GCB cells irrespective of *Cfp1* status, confirming the distinct functional properties of this compartment (Fig. S12A). In addition, FACS analysis with two additional surface panels, pre-MBC #2 B220$^+$IgD$^-$CD95$^+$GL7$^+$Efnb1$^+$CD38$^+$CXCR4^{lo} and #3 B220$^+$IgD$^-$CD95$^+$GL7$^+$CD86^{hi}CXCR4^{lo}CCR6$^+$ (Fig. S11C), revealed similarly expanded pre-MBCs in *Cfp1*-deficient mice (Fig. 7B, C).

To investigate whether *Cfp1* loss promotes memory B cell formation through regulating the expression of pre-MBC genes, we analyzed our mRNA-seq data with a reported pre-MBC geneset by GSEA[61]. The result showed a strong enrichment of pre-MBC genes in *Cfp1*$^{fl/fl}$*Aicda*^{Cre} GCB cells (Fig. 7D). Moreover, H3K4me3 signal intensity at the promoter region of pre-MBC signature genes was markedly increased in *Cfp1*-deficient cells (Fig. 7E). Examining H3K4me3 signals of the pre-MBC genes with altered expression, we discovered that 104 (38%) differentially expressed pre-MBC signature genes exhibited increased H3K4me3 marks at the promoters (Fig. S12B). For instance, *Hhex* and *Bcl2* which have been shown as pre-MBC genes[12], were significantly upregulated at both the mRNA level and H3K4me3 marks in *Cfp1*-knockout GCB cells (Fig. 7F). Interestingly, we found that 24% (66/274) of pre-MBC genes were regulated by bivalent promoters, among which 58% (38/66) fell into the both up group (Fig. S12C), implicating that redistribution of H3K4me3 to bivalent genes upon *Cfp1* loss could play an active role in pre-MBC gene activation and memory B cell differentiation.

Bcl6 has been shown to suppress genes crucial for MBC development[31]. As *Cfp1* deletion markedly downregulated *Bcl6*, we

https://doi.org/10.1038/s41467-025-63291-8

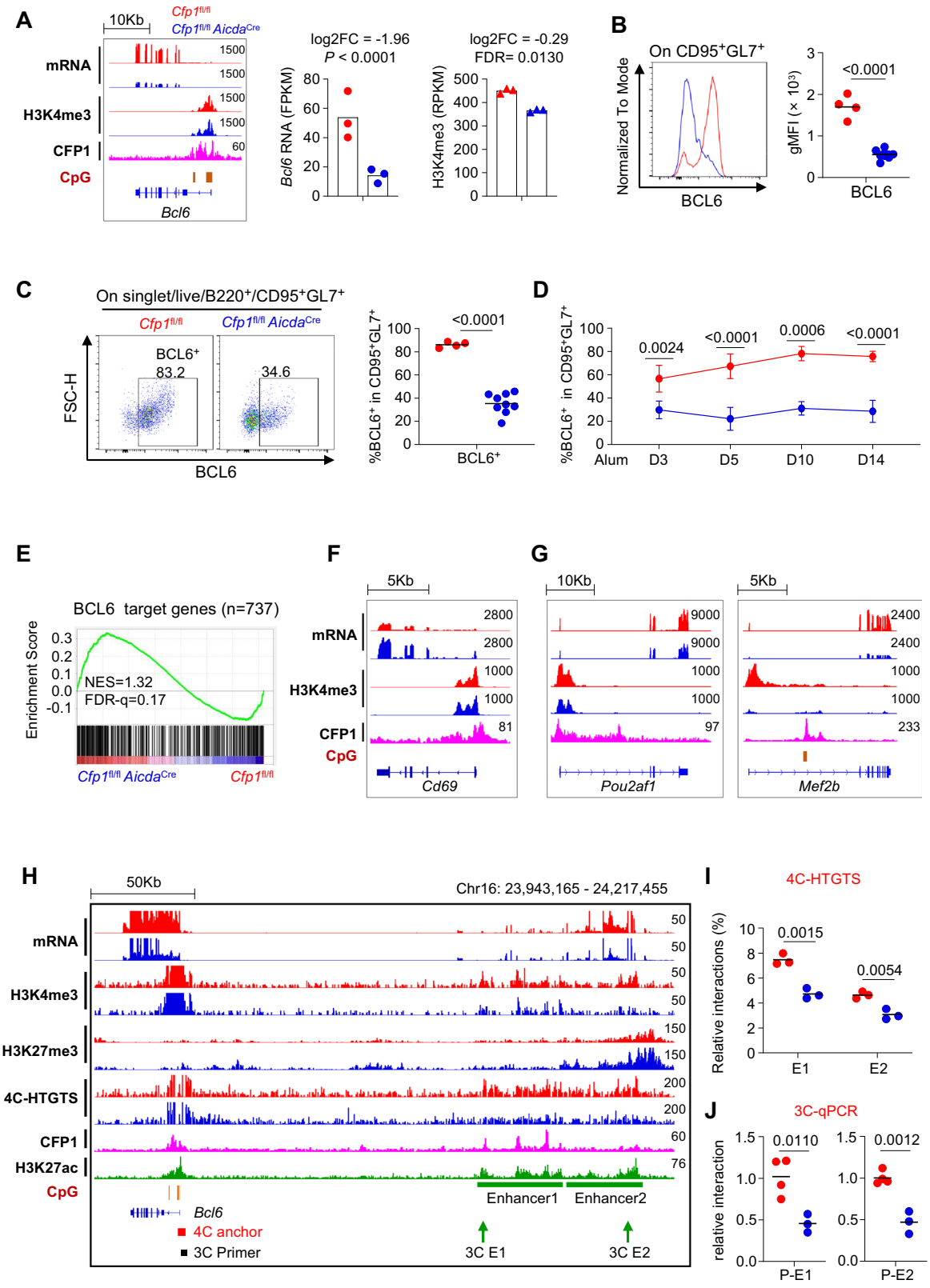

asked whether H3K4me3-reglated transcription or *Bcl6* per se affected the expression of pre-MBC genes. To this end, we intersected *Bcl6* target genes in GCB cells with the pre-MBC signature genes and the genes exhibiting both up in mRNA and H3K4me3 levels following *Cfp1* loss. Among the 274 pre-MBC signature genes, 51 (18.6%) were *Bcl6* targets and 64 (23.3%) overlapped with both up genes, among which 23 were also *Bcl6* targets, including *Hhex, Bcl2, Zeb2, Cdkn1b, S1pr1*, etc. (Fig. 7G, H; Fig. S12D and Supplementary data 3). The pre-MBC signature genes that are not *Bcl6* target genes but exhibited both up in mRNA and H3K4me3 levels in *Cfp1*$^{fl/fl}$*Aicda*^{Cre} GCB cells included *Ccr6, Bhlhe40, Gpr65, Runx3*, etc (Fig. 7G, H; and Fig. S12E). We concluded that downregulation of *Bcl6* and upregulation of H3K4me3 in the absence of *Cfp1* cooperatively contributed to the induction of the pre-MBC signature genes.

Fig. 4 | CFP1 is critical for BCL6 expression in GC B cells. Mice were immunized with NP-KLH/MnJ, boosted on day 8 and analyzed on day 14 except for (**D**). **A** Genome browser plot for *Bcl6* gene showing mRNA and occupancy of indicated factors in control and *Cfp1*$^{fl/fl}$*Aicda*^{Cre} GCB cells (left). Bar plots showing *Bcl6* mRNA expression (log2FC, *P*-value; DESeq2) and *Bcl6* H3K4me3 signal (log2FC, FDR; Diffbind) (right); $n = 3$; 3 females (f) for mRNA; 1 males (m), 2 f for H3K4me3. **B** Geometric mean of fluorescence intensity (gMFI) of intracellular BCL6 in control and *Cfp1*$^{fl/fl}$*Aicda*^{Cre} GCB cells. Data were pooled from two independent experiments; *Cfp1*$^{fl/fl}$ ($n = 4$; 2 m, 2 f); *Cfp1*$^{fl/fl}$ *Aicda*^{Cre} ($n = 9$; 4 m, 5 f). $p < 0.0001$ (= 2.48e−7). **C** Percentage of splenic BCL6$^+$ cells within GCB (B220$^+$CD95$^+$GL7$^+$) in control and *Cfp1*$^{fl/fl}$*Aicda*^{Cre} mice. Data were pooled from two independent experiments; *Cfp1*$^{fl/fl}$ ($n = 4$; 2 m, 2 f); *Cfp1*$^{fl/fl}$ *Aicda*^{Cre} ($n = 9$; 4 m, 5 f). $p < 0.0001$ (= 2.64e−7). **D** Mice were immunized with NP-KLH/Alum and analyzed at indicated time points. The ratio of BCL6$^+$ cells in total splenic GCB cells at different time points after immunization were shown. Data were pooled from three independent experiments; *Cfp1*$^{fl/fl}$ (Day3 $n = 4$; 2 m, 2 f; Day5 $n = 5$; 2 m, 3 f; Day 10/14 $n = 3$; 2 m, 1 f); *Cfp1*$^{fl/fl}$ *Aicda*^{Cre} (Day3 $n = 5$; 2 m, 3 f; Day5 $n = 9$; 4 m, 5 f; Day10 $n = 3$; 1 m, 2 f; Day14 $n = 6$; 3 m, 3 f). $p < 0.0001$ (D5 = 1.26e−6, D14 = 9.20e−5). **E** GSEA analysis for BCL6 target gene expression in *Cfp1*$^{fl/fl}$ and *Cfp1*$^{fl/fl}$*Aicda*^{Cre} cells. **F** Genome browser view of *Cd69* mRNA and H3K4me3 in control and *Cfp1*-deficient GCB cells. **G** Genomebrowser plots of *pou2af1* and *mef2b* as in (F). **H** Genomebrowser view for mRNA, H3K4me3, H3K27me3, 4C interaction, CFP1 and H3K27ac (green: wild type) of *Cfp1*$^{fl/fl}$ and *Cfp1*$^{fl/fl}$*Aicda*^{Cre} GCB cells at *Bcl6* locus were shown. H3K27Ac[81] track was used to position enhancer cluster. Relative interaction frequency (Reads in this region/total reads) measure by the 4C-HTGTS **I** and confirmation by 3C-qPCR **J** for interaction between *Bcl6* promoter and enhancers. Data were pooled from two independent experiments; 4C-HTGTS: $n = 3$; 1 m, 2 f; 3C-qPCR: *Cfp1*$^{fl/fl}$ ($n = 4$; 2 m, 2 f); *Cfp1*$^{fl/fl}$ *Aicda*^{Cre} ($n = 3$; 1 m, 2 f). **B**, **C** and **H**, **I**) Each symbol indicates one mouse and lines denote means. **D** Data points represent the mean ± SD. *P*-values by unpaired *t*-test (two-tail). Genome browser plots (red and purple: *Cfp1*$^{fl/fl}$; blue: *Cfp1*$^{fl/fl}$*Aicda*^{Cre}).

Discussion

Our study revealed the critical roles of *Cfp1* in germinal center dynamics, affinity maturation, and terminal differentiation. In a working model (Fig. 8) we propose that in the absence of *Cfp1*, antigen-activated B cells fail to proliferate robustly and tend to differentiate into extrafollicular memory B cells. Those *Cfp1*-deficient B cells indeed forming germinal centers are prone to exit pre-maturely to preferentially differentiate into MBCs and PCs with diminished affinities (Fig. 8A). At the molecular levels, *Cfp1* positively regulates the transcription, likely through H3K4me3 modification, of cell cycle genes to safeguard robust proliferation of both extrafollicular and intrafollicular cells (Fig. 8B, upper panel). In addition, CPF1 governs GC entry and maintenance by regulating MEF2B/OCA-B and chromatin looping-mediated *Bcl6* induction. In the absence of *Cfp1*, markedly reduced BCL6 derepresses IRF4 to increase differentiation into PCs (Fig. 8B, middle). Combined with transcriptional upregulation conferred by elevated H3K4me3 marks, downregulated *Bcl6* expression also leads to the significant upregulation of pre-MBC genes *Hhex, Ccr6, Bcl2*, etc. that collectively favor GCB differentiation into memory B cells (Fig. 8B, lower panel). *Cfp1* regulates each step of the germinal center B cell response either directly or indirectly through H3K4me3 modifications.

Unlike transcription factors whose roles in GC reactions are fairly well understood, the dynamics epigenetic landscape in GC response is still elusive. Earlier reports revealed that histone methyltransferase EZH2 is required for GC formation by depositing the repressive mark H3K27me3[35,62]. Gain-of-function (GOF) mutations in EZH2 with hyperactive H3K27me3, often found in the GCB-type of DLBCLs, enhance cell proliferation through greater repression of CDKN1A[35,63]. Our work represents another example of epigenetic modification with pivotal roles in GC maintenance. *Cfp1* positively regulates key cell cycle genes for proper S phase entry. As a result, *Cfp1*-deficient GCB cells exhibit severely impaired proliferation, suggesting that both active and repressive histone modifications, acting on positive and negative regulators of the cell cycle, respectively, are required for the robust proliferation of germinal center B cells.

It appears that *Cfp1* is differentially required for H3K4me3 implementation in cells with different differentiation status. *Cfp1* plays a much more important roles in H3K4me3 deposition in germ cells as its deletion significantly reduces global levels of this mark[64,65]. In mES cells although global H3K4me3 is not affected by *Cfp1* loss, more than 50% of its association peaks were reduced[18]. In this study, *Cfp1* deletion in GCB caused slightly higher H3K4me3 association in the genome with nearly one-third of peaks gaining signals. Therefore, the requirement for *Cfp1* to install H3K4me3 marks appears gradually decreasing as cells become more differentiated. Similar changing requirements of MLL2 for global H3K4me3 implementation in oocytes but much less so in later development have been documented[66,67]. In addition, *Cfp1* has been reported to restrain ectopic H3K4me3 at certain enhancers in mES cells[18]. We found redistribution of H3K4me3 from active genes to bivalent promoters, but not enhancers, in GCB cells with *Cfp1* deletion. This observation is consistent with another recent report in oocyte where *Cfp1* deletion causes elevated H3K4me3 and suppressed H3K27me3 at subset of bivalent genes for their upregulation[68]. The phenotype discrepancy suggests cell type or differentiation stage-specific mechanisms to regulate genome-wide distribution of H3K4me3. Our finding also suggests that H3K4 HMTs other than Setd1A/B can efficiently complement the loss of *Cfp1* in GCB cells, or alternatively, *Cfp1*-independent recruitment of the Setd1A/B complex to genome sites[19].

It is still debatable whether H3K4me3 plays instructive roles in transcription. Deletion of *Cfp1* in mES cells[18] or its budding yeast ortholog *Spp1*[69] did not cause major transcriptional changes despite reduced H3K4me3, arguing against an instructive role. We found the *Cfp1* deletion in GCB cells did not significantly impact global gene transcription, consistent with the findings in mES cells[18]. However, we indeed found that cell cycle and a subset of GCB-related genes were significantly reduced with concomitant reduction in H3K4me3 levels. Further analysis revealed that these genes are actively transcribed at high levels. It is likely that highly expressed genes could serve as reservoirs, probably through unmethylated CpG islands in the promoter[20], to recruit and contain *Cfp1*-associated HMT activity. In addition, recent studies revealed that H3K4me3 promotes transcription elongation through releasing RNA polymerase II from the promoter-proximal regions[70,71]. The lack of impact on genome wide Pol II association and pausing in *Cfp1*-deficient GCB cells do not necessarily contradict with this model as *Cfp1* deletion does not interfere with the global H3K4me3. That being said, we cannot exclude the possibility that at certain specific locales with altered H3K4me3, *Cfp1* loss may still affect Pol II recruitment or pausing for their transcription modulation.

One of the most prominent target genes of *Cfp1* is *Bcl6* that is crucial for GC entry and maintenance[3]. Promoting the expression of key upstream transcription factors MEF2B and OCA-B likely through H3K4me3 modification, *Cfp1* is required for *Bcl6* expression through the looping of *Bcl6* promoter and enhancers that critically depends on MEF2B and OCA-B binding. In addition, *Bcl6* has been shown to be tightly regulated at the transcription level by T cell-derived cytokines IL-4 and IL-21[8,9,47,50] that derepress the *Bcl6* locus by demethylating H3K27me3 at the enhancers. We found that *Cfp1* deletion caused markedly increased H3K27me3 levels accompanied with reduced H3K4me3 and eRNA at the enhancers. Our study thus updated the regulatory modes of *Bcl6* transcription through upstream regulators and the epigenetic modification of its enhancers by *Cfp1*. *Bcl6* deficiency in the absence of *Cfp1* can largely explain the failed GC entry, in addition to diminished cell proliferation and the maintenance of the germinal center. Biased differentiation of GCB into plasma cells upon

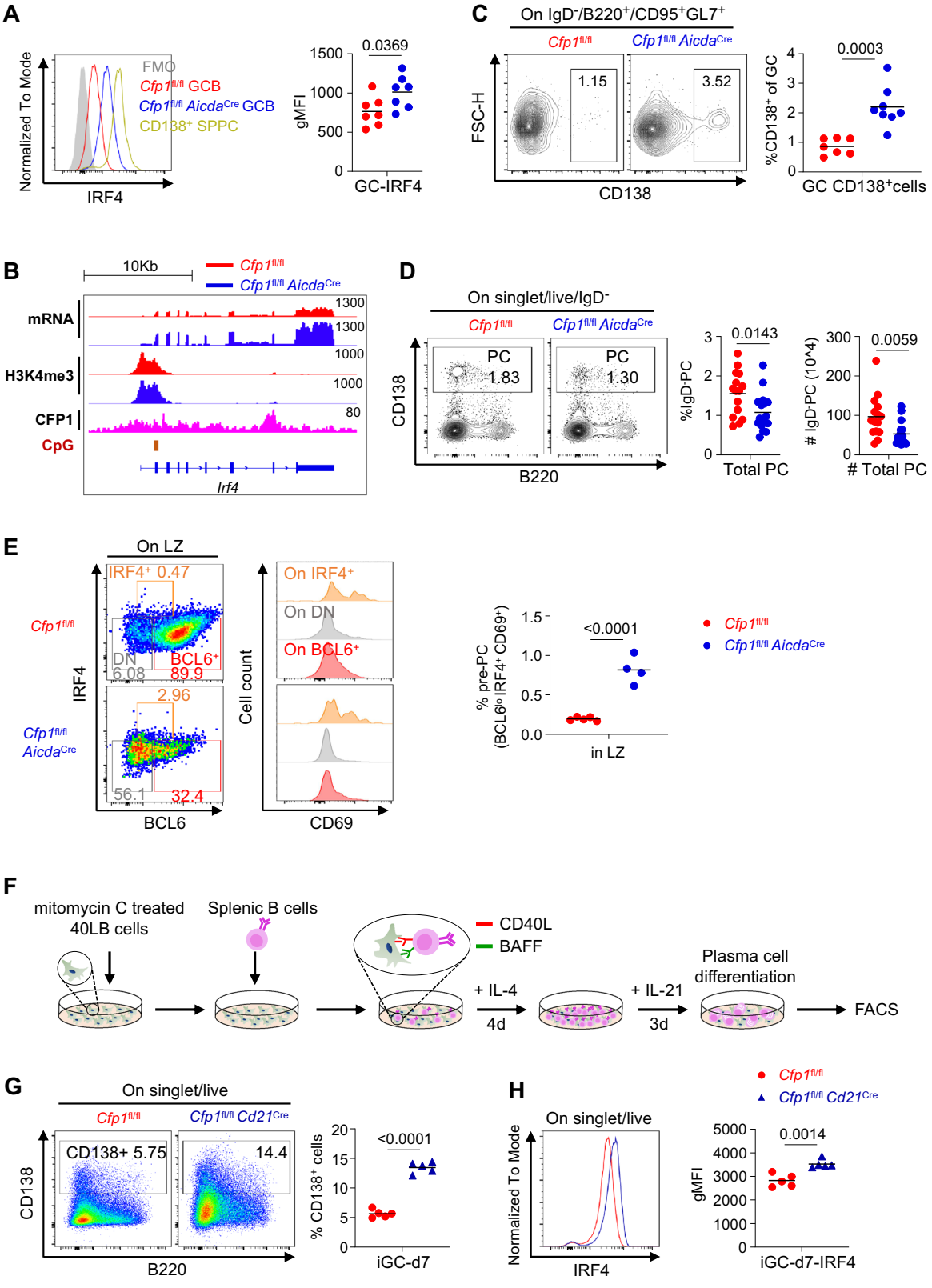

Cfp1 loss can also be attributed to deficient *Bcl6* induction that derepresses *Irf4*.

Bcl6 downregulation may also contribute to the preferred differentiation of *Cfp1*-deficient GCB cells into memory B compartment, as the cease of *Bcl6*-mediated transcriptional suppression has been shown to drive pre-MBC gene expression[31]. However, as most pre-MBC genes are not *Bcl6* targets, *Bcl6* independent mechanisms should exist for their induction. An earlier report suggested that subsets of MBC genes are under control by bivalent promoters. Supporting this notion, the EZH2^{Y641F} GOF mutation reduces MBC signature gene expression and confers diminished memory B differentiation[35]. We confirmed the regulation of a subset of pre-MBC genes by bivalent promoters. In addition, our work suggests that redistribution of H3K4me3 from active genes to bivalency-controlled

Fig. 5 | *Cfp1* deletion promotes differentiation of GCB into plasma cells. Mice were immunized with NP-KLH/MnJ, boosted on day 8 and analyzed on day 14. **A** Intracellular staining (red and yellow: *Cfp1*$^{fl/fl}$; blue: *Cfp1*$^{fl/fl}$ *Aicda*^{Cre}) and gMFI of IRF4 in control and *Cfp1*$^{fl/fl}$*Aicda*^{Cre} GCB cells in the spleen. Data were pooled from two independent experiments; $n = 7$; 3 m, 4 f. FMO, Fluorescence Minus One. **B** Genomebrowser view of the *Irf4* mRNA, H3K4me3 and CFP1 occupancy (red and purple: *Cfp1*$^{fl/fl}$; blue: *Cfp1*$^{fl/fl}$ *Aicda*^{Cre}) in control and *Cfp1*-deficient GCB cells. **C** Ratio of CD138$^+$ cells over GCB (IgD$^-$B220$^+$CD95$^+$GL7$^+$) cells in the spleen of control and *Cfp1*-deficient mice. Data were pooled from three independent experiments; *Cfp1*$^{fl/fl}$ ($n = 7$; 3 m, 4 f); *Cfp1*$^{fl/fl}$ *Aicda*^{Cre} ($n = 8$; 4 m, 4 f). **D** Ratio and absolute numbers of plasma cells (IgD$^-$CD138$^+$) over total splenic B cells. Data were pooled from five independent experiments; *Cfp1*$^{fl/fl}$ ($n = 15$; 6 m, 9 f); *Cfp1*$^{fl/fl}$ *Aicda*^{Cre} ($n = 17$; 8 m, 9 f). **E** Representative flow cytometry (orange: IRF4$^+$; red: BCL6$^+$; grey: IRF4$^-$BCL6$^-$) to identify PC precursors (BCL6^{lo} IRF4$^+$ CD69$^+$) in LZ GCB (B220$^+$IgD$^-$GL7$^+$CD38$^-$CD86^{hi}CXCR4^{lo}). Data were pooled from two independent experiments; *Cfp1*$^{fl/fl}$ ($n = 5$; 2 m, 3 f); *Cfp1*$^{fl/fl}$ *Aicda*^{Cre} ($n = 4$; 2 m, 2 f). $p < 0.0001$ (= 9.16e−5). **F** Schematic illustration of in vitro iGCB induction and plasma cell differentiation with the 40LB culture system. **G** Flow cytometry plots and ratio of CD138$^+$ PC on 40LB cultures supplemented with IL-4 and subsequent IL-21 for 3 additional days. Data were pooled from two independent experiments; $n = 5$; 1 m, 4 f. $p < 0.0001$ (= 3.64e−7). **H** Intracellular staining and gMFI (red: *Cfp1*$^{fl/fl}$; blue: *Cfp1*$^{fl/fl}$*Cd21*^{Cre}) of IRF4 in control and *Cfp1*$^{fl/fl}$*Cd21*^{Cre} iGCB cells. Data were pooled from two independent experiments; $n = 5$; 1 m, 4 f. **A**–**H** Each symbol indicates one mouse and lines denote means. *P*-values by unpaired *t*-test (two-tail).

pre-MBC genes in GCB cells could play an important role to activate these genes to initiate memory B differentiation. It remains to be determined the responsible HMT activity to deposit H3K4me3 at bivalent promoters in the absence of *Cfp1*, and how *Cfp1*-associated Setd1A/B dynamically interplays with this particular HMT for proper H3K4me3 installation at the bivalency regions in a wild-type GC. In this regard, Mll2/KMT2B has been shown to catalyze H3K4me3 at bivalent promoters in ES cells[72,73]. It is therefore of interest to investigate whether Mll2 plays any role in primary GC and MBC differentiation as well as recall responses.

Additionally, our study revealed that *Cfp1* loss leads to the upregulation of subsets of innate immune response, cytokine signaling, inflammatory response, and chemotaxis genes accompanied by elevated H3K4me3. A very recent report indicated that inflammatory factors actively impede germinal center response, which can be partially rescued by inhibition of the IL-1 signaling pathway. This study highlighted the critical roles of chromatin modeling complex in suppressing inflammatory gene expression for efficient GC reactions. Our study extended this observation by showing that specific H3K4me3 programs mediated by *Cfp1* restrain the negative impact of inflammatory genes on the ongoing GC response.

In summary, our study revealed that directly or indirectly through implementing H3K4me3 marks at subsets of genes, *Cfp1* regulates GC commitment, dynamics, and terminal differentiation of GCB cells. As altered proliferation and differentiation of GCB are often seen in mature B cell lymphomas, the insights obtained in this study may also help elucidate the mechanisms of lymphomagenesis driven by interruptions in GCB-specific epigenetic programs.

Methods

Mice

All mice were crossed onto C57BL/6J (stock No.000664) background and housed under specific-pathogen-free (SPF) conditions at the animal facility of the Laboratory Animal Center of Sun Yat-sen University. All animal experiments were carried out with approval from the Animal Care and Ethics Committee of Sun Yat-sen University (SYSU-IACUC). All mouse experiments were performed on 8–12 week old mice housed under SPF conditions at 22 ± 1 °C and 50–60 % humidity with a 12 h light/dark cycle. The following mouse strains on a C57BL/6J background were used: *Cfp1*$^{fl/fl}$[24], *Cd21*^{Cre}[25], and *Aicda*^{Cre}[30].

Mice were euthanized by CO_2 anesthetized using the Quietek™ system (ensuring proper flow rate and chamber fill volume) followed by confirmatory cervical dislocation, in full compliance with IACUC guidelines. The study utilized both male and female mice in all experiments. To maintain gender balance, control and experimental groups were systematically sex-matched whenever possible. While sex was not included as an independent variable in data analysis, complete sex information is comprehensively documented in the corresponding figure legends.

Immunization and treatments

For immunization with alum adjuvant, mice were immunized intraperitoneally with 100 µg of NP-KLH (N-5060-25, Biosearch Technologies) precipitated with 100 µl alum adjuvant (77161, Thermo Scientific). For immunization with MnJ adjuvant, mice were immunized intraperitoneally with 60 µg of NP-KLH mixed with 300 µg MnJ (MS0001, MnStarter Biotechnology) and boosted with 60 µg NP-KLH at day 8 for analysis at day 14. For immunization with SRBC, 20 ml sterile SRBCs (BJLY10031, NJlezhen Biotechnology) were washed twice with 30-50 ml ice-cold PBS and reconstituted in 5 ml PBS and mice were immunized intraperitoneally with 0.1 ml and boosted with 0.2 ml at day 5 for analysis at day 12.

Flow cytometry and cell sorting

Bone marrow cells were flushed from tibias and femurs and spleens were mashed. Bone marrow cells and splenocytes were filtered through 40 or 70-µm cell strainers, respectively. RBCs were lysed by resuspending in 3 ml RBC Lysis Buffer (R1010-500, Solarbio) for 5 min on ice. Dead cells were excluded from analysis based on staining with Zombie Near IR (1/1000 dilution, 423106, Biolegend) in PBS for 30 min on ice, followed by Fc Block (1/50 dilution, 553142, BD Biosciences) for 15 min and surface antibodies for 30 min in FACS buffer (PBS supplemented with 2% FBS and 2 mM EDTA) on ice.

For intracellular staining (a-Caspase3), cells were fixed and permeabilized by Cytoperm/Cytofix kit (554714, BD Biosciences) according to the provided protocol. For transcription factor (BCL6, IRF4, KI67) staining, cells were fixed and permeabilized by a transcription factor staining kit (00-5521-00, eBioscience).

For in vivo cell cycle analysis, 2 mg BrdU (HY-15910, MCE) was injected intraperitoneally and mice were sacrificed after 2 h. Splenocytes were harvested and stained with viability dye (Zombie Near IR) and antibodies against the surface marker, fixed and permeabilized then labeled using APC BrdU Flow kit (552598, BD Biosciences) according to the provided protocol, treated with DNase I (300 µg/ml) for 1 h at 37 °C, and stained intracellularly with APC-conjugated anti-BrdU antibody (1/50 dilution, 364114, Biolegend) for 30 min. Before analysis, resuspend the cells in 7AAD (1/100 dilution, 420404, Biolegend) solution to indicate DNA content. All cytometric data were collected on the Cytoflex/Cytoflex S Flow Cytometer (Beckman Coulter) and analyzed with the FlowJo software (Version 10.8.1).

For in vivo pre-memory B cells EdU incorporation assay, 0.75 mg EdU (HY-118411, MCE) was injected intraperitoneally and mice were sacrificed after 2.5 h. Splenocytes were stained with viability dye and antibodies against the surface marker, fixed and permeabilized by Cytoperm/Cytofix kit according to the provided protocol, then EdU staining kit (C10371-1, RIBOBIO) was used. All cytometric data were collected on the Cytoflex/Cytoflex S Flow Cytometer (Beckman Coulter) or on the Cytek Aurora and analyzed with the FlowJo software (Version 10.8.1).

Niave B cells were isolated using the EasySep Mouse B Cell Isolation Kit (19854A, Stemcell Technologies) according to the

https://doi.org/10.1038/s41467-025-63291-8

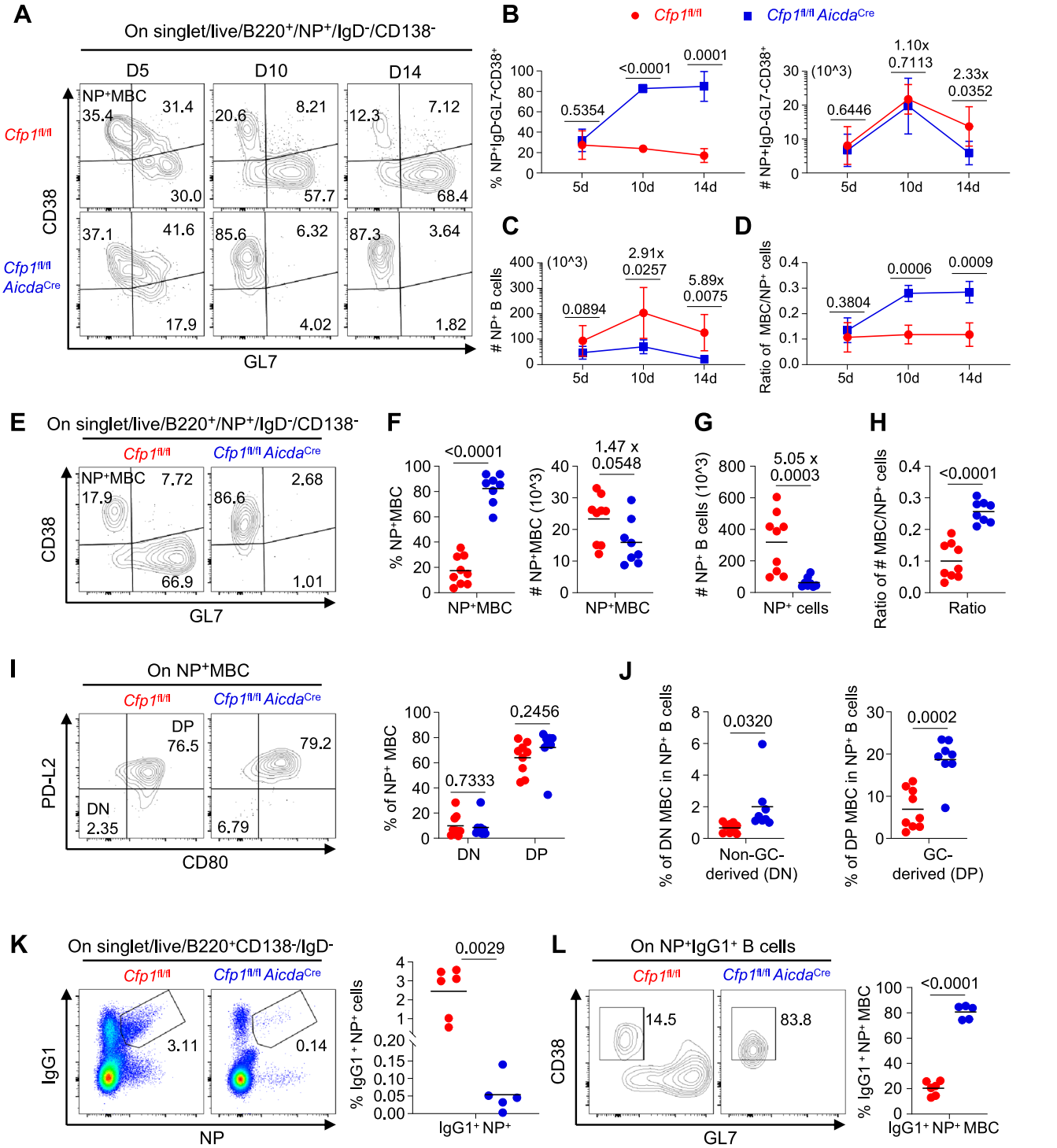

Fig. 6 | *Cfp1*-deficient GCB cells have greater propensity to differentiate into memory B cells. A–D Mice were immunized with NP-KLH/Alum and analyzed at indicated time points. Data were pooled from three independent experiments; *Cfp1*$^{fl/fl}$ (Day5 $n = 5$; 2 m, 3 f; Day 10/14 $n = 3$; 1 m, 2 f); *Cfp1*$^{fl/fl}$ *Aicda*^{Cre} (Day5 $n = 7$; 4 m, 3 f; Day10 $n = 5$; 2 m, 3 f; Day14 $n = 6$; 3 m, 3 f). **E–L** Mice were immunized with NP-KLH/MnJ, boosted on day 8 and analyzed on day 14 p.i. Data were pooled from three independent experiments; *Cfp1*$^{fl/fl}$ ($n = 9$; 4 m, 5 f); *Cfp1*$^{fl/fl}$ *Aicda*^{Cre} ($n = 8$; 4 m, 4 f). **A** FACS plots and **B** ratio (left) and absolute numbers (right) of NP$^+$ memory B cells (CD38$^+$GL7$^-$) within non-plasma cells compartment (B220$^+$NP$^+$IgD$^-$CD138$^-$). $p < 0.0001$ (10d = 6.57e−7). **C** Absolute numbers of NP$^+$ B cells (B220$^+$NP$^+$). **D** The ratio of NP$^+$ memory B cells to NP$^+$ B cells is shown. **E** FACS plots and **F** ratio (left) and absolute numbers (right) of NP$^+$ memory B cells within non-plasma cells compartment. $p < 0.0001$ (=7.31e−9). **G** Absolute numbers of NP$^+$ B cells. **H** The ratio of NP$^+$ memory B cells to NP$^+$ B cells is shown. $p < 0.0001$ (=6.42e−6). **I** Representative FACS plots (left) and ratio (right) of CD80$^+$PDL2$^+$ DP and CD80$^-$PDL2$^-$ DN subsets among NP$^+$MBC. **J** Ratio of GC-derived (DP) and non-GC-derived (DN) memory B cells in total NP$^+$ B cells. FACS plots and ratio of **K** IgG1$^+$NP$^+$ B cells, **L** IgG1$^+$NP$^+$ memory B cells of *Cfp1*$^{fl/fl}$ and *Cfp1*$^{fl/fl}$*Aicda*^{Cre} mice. Data were pooled from two independent experiments; *Cfp1*$^{fl/fl}$ ($n = 6$; 3 m, 3 f); *Cfp1*$^{fl/fl}$ *Aicda*^{Cre} ($n = 5$; 2 m, 3 f). $p < 0.0001$ (=2.32e−8). **B–D** Data points represent the mean ± SD. **F–L** Each symbol indicates one mouse and lines denote means. Numbers indicate fold-changes (shown as 1.10x, 2.33x, etc.) in mean cell counts with *p*-values above. *P*-values by unpaired *t*-test (two-tail).

https://doi.org/10.1038/s41467-025-63291-8

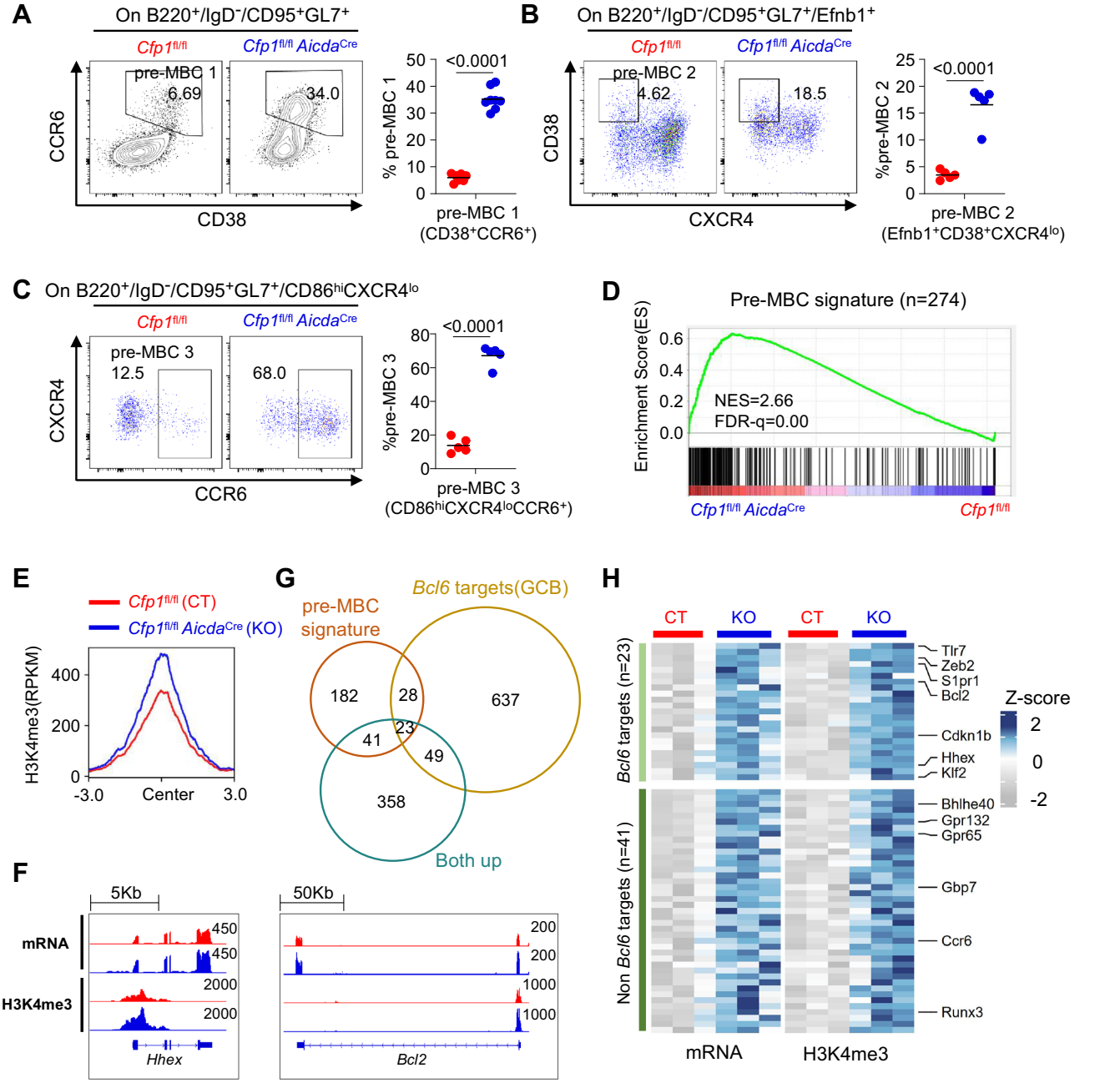

Fig. 7 | *Cfp1* deletion promotes pre-MBC gene expression. A–G Mice were immunized with NP-KLH/MnJ, boosted on day 8 and analyzed on day 14. FACS plots and ratio of memory B cell precursors (pre-MBC) defined by **A** CD38$^+$CCR6$^+$, *Cfp1*$^{fl/fl}$ ($n = 7$; 4 m, 3 f); *Cfp1*$^{fl/fl}$ *Aicda*^{Cre} ($n = 8$; 4 m, 4 f), **B** Efnb1$^+$CD38$^+$CXCR4^{lo}, n = 5; 2 m, 3 f and **C** CD86^{hi}CXCR4^{lo}CCR6$^+$, n = 5; 2 m, 3 f. Data were pooled from two independent experiments. (pre-MBC1 = 1.49e−10, pre-MBC2 = 5.20e−5, pre-MBC3 = 2.15e−7). **D** GSEA analysis for pre-memory signature genes in control and *Cfp1*$^{fl/fl}$*Aicda*^{Cre} GCB cells. $p < 0.0001$. **E** Comparison of H3K4me3 signal around peak center (±3 kb) at pre-MBC gene promoters in control and *Cfp1*$^{fl/fl}$*Aicda*^{Cre} GCB cells (red: *Cfp1*$^{fl/fl}$; blue: *Cfp1*$^{fl/fl}$*Cd21*^{Cre}). **F** Genomebrowser tracks for mRNA and H3K4me3 of *Hhex* and *Bcl2* genes in *Cfp1*$^{fl/fl}$ and *Cfp1*$^{fl/fl}$*Aicda*^{Cre} GCB cells. **G** Venn diagram showing the overlap between pre-MBC signature genes, *Bcl6* target genes and Both up genes. **H** Heatmap for the mRNA and H3K4me3 signals of upregulated pre-MBC genes upon *Cfp1* loss. **A–C** Each symbol indicates one mouse and lines denote means. *P*-values by unpaired *t*-test (two-tail).

manufacturer's instructions. For GL7$^+$ B cells (B220$^+$GL7$^+$)/GCB cells (B220$^+$CD95$^+$GL7$^+$) sorting from spleen, cell suspensions were prepared and stained with Zombie Near IR, B220-APC, GL7-FITC and CD95-PE. The cells were sorted by FACSAria III (BD) or MoFlo Astrios (Beckman). Gating strategies used for cell sorting are shown in Supplementary Fig. 14.

Antibodies are listed in Supplementary Table 2. A universal 1/500 dilution was maintained for all antibody-based assays, with exceptions stated in the Method.

In vitro proliferation assay

Splenic naïve B cells were isolated using the EasySep Mouse B Cell Isolation Kit (19854A, Stemcell Technologies) according to the manufacturer's instructions. Purity validated by flow cytometry was more than 95%. Splenic naïve B cells isolated as above were cultured at 5×10^5 cells/ml in the B cell medium RPMI-1640 (10040-CV, Corning) supplemented with 15% FBS (FSP500, ExCellBio), 1× penicillin/streptomycin (30-002-CI,Corning), 20 mM HEPES buffer (25-060-CI, Corning), 2 mM L-Glutamine (25-005-CI, Corning) and 1 mM sodium

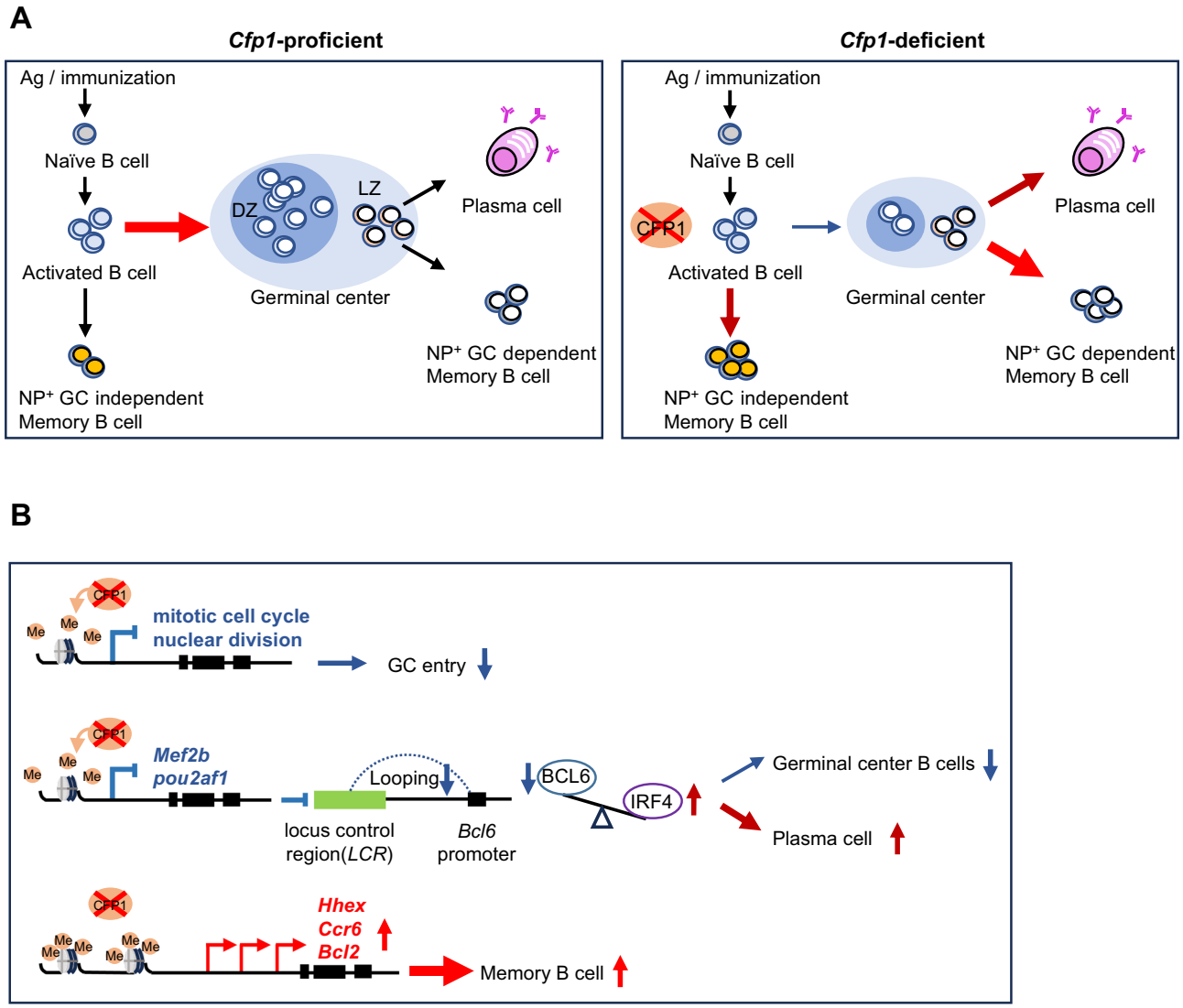

Fig. 8 | Proposed model by which CFP1 regulates GC responses. A *Cfp1* deficiency impairs GC commitment and leads to premature exit of GCB cells to differentiate into plasma cells and memory B cells. **B** Molecular mechanisms of *Cfp1*-mediated regulation of GC response through expression of GCB-related genes indirectly or directly through H3K4me3 modification. See text for details.

pyruvate (25-000-CI, Corning), 1× MEM nonessential amino acids (25-025-CI, Corning), and 50 μM β-mercaptoethanol (0482, Amresco) and were treated with 0.5 μg/ml anti-CD40 (14-0402-86, eBioscience), 50 ng/ml IL-21 (210-21, Peprotech) and 20 ng/ml IL-4 (96-214-14, Peprotech) for 48 h at 37 °C with 5 % CO_2, then cells were collected and fixed with ice-cold 70% methanol at −20 °C for 3 h, treated with 10 μg/ml RNase A for 30 min at 37 °C, and then resuspended in PBS supplemented with 50 μg/ml PI (P4868, Sigma-Aldrich) to indicate DNA content. For the proliferation assay, splenic naïve B cells were stained with CellTrace CFSE (1/1000 dilution, C34570, Invitrogen) according to the manufacturer's instructions. Cells were seeded and stimulated as above. Data were collected on the Cytoflex Flow Cytometer (Beckman Coulter) and analyzed with the CytExpert (Version 2.3.1).

Western blot

To extract whole-cell lysates, at least 1×10^5 cells were collected and washed once with ice-cold PBS and resuspended in 1% SDS buffer (50 mM Tris-HCl pH 8.0, 10 mM EDTA, 1%SDS) supplemented with 1 mM protease inhibitors PMSF and incubated on ice for 10 min. Lysates were separated by 12% Bis-Tris precast gels. After electrophoretic transfer to Immobilon PVDF membrane (IPVH00010, Millipore), membranes were blocked the 5% non-fat milk in PBS containing 0.1% Tween-20. Membranes were incubated overnight at 4 °C with the following primary antibodies: Rabbit CFP1 (1/3000 dilution, Anti-CGBP, ab198977, Abcam), Mouse β-actin (1/5000 dilution, 66009-1-Ig, proteintech). Membranes were then incubated with HRP-conjugated anti-rabbit secondary antibody (1/3000 dilution, SA00001-2, proteintech) or anti-mouse secondary antibody (1/3000 dilution, 7076, Cell Signaling Technology) and detected by ChemiDoc Touch Imaging System (Bio-Rad).

Droplet digital PCR analysis

Genomic DNA was extracted from FACS-sorted splenic GCB cells via phenol-chloroform method. Each 20-μl reaction contained: 10 μl of 2 × EvaGreen ddPCR Master Mix (S0200020302, Forevergen), 1 μl of forward primer and 1 μl of reverse primer (10 μM each), 2 μl template DNA, and 6 μl nuclease-free water. Droplets were generated using MicroDrop-100A (Forevergen). Samples were amplified in the ETC811 Thermal Cycler (Eastwin) according to the following steps: 95 °C for 10 min, 40 cycles of 95 °C for 30 s and 60 °C for 60 s, and 72 °C for 2 min. The amplified droplets were detected in a MicroDrop-100B Droplet Reader (Forevergen) and the DNA concentration (copies/μl) of

each sample was calculated with QuantDrop analysis software (Forevergen) following the principle of the poisson distribution. The *Cfp1* copies were calculated by normalizing *Cfp1* concentration to the reference gene *Gapdh* (2 copies/diploid cell) using the formula: *Cfp1* copies/cell = (*Cfp1* copies/μl) / (*Gapdh* copies/μl) × 2. The relative copies of *Cfp1* was normalized to the mean value of $Cfp1^{fl/fl}$ mice. Primers for ddPCR are listed in Supplementary Table 1.

qPCR

Genomic DNA was extracted by phenolchloroform. The ChamQ Universal SYBR qPCR Master Mix (Q711, Vazyme) was used to set up SYBR Green-based quantitative PCR reactions following the manufacturer's protocol. Samples were analyzed on a CFX Connect Real-Time system (Bio-Rad) and melting curves were used to validate correct amplification products. DNA levels of *Cfp1* were normalized to generic housekeeping gene *Gapdh*. Primers for qPCR are listed in Supplementary Table 1.

ELISA

Following immunization with MnJ adjuvant, Mouse serum samples were collected at day 14 after immunization for NP-specific assays, ELISA plates (9018, Corning) were coated with 100 μl 5 μg/ml NP_{32}-BSA (N-5050H-10, Biosearch Technologies) or NP_2-BSA (N-5050L-10, Biosearch Technologies) overnight at 4 °C. Plates were washed 3 times with 0.05% PBST, loaded with 100 μl diluted serum samples per well and incubated for 2.5 h at 37 °C. Plates were washed 6 times with PBST and secondary antibodies were added for detecting IgG1 (1071-05, SouthernBiotech) for 1.5 h at 37 °C. After washed 6 times, 100 μl of TMB substrate (PR1200, Solarbio) was added to each well to develop for 60–120 s, and 100 μl 1 M H_2SO_4 was used to stop the reaction. Plates were read at 450 nm by using Tecan's Sunrise absorbance microplate reader.

iGC B cell culture

For in vitro expansion and differentiation of B cells, 40LB feeder cells[29] expressing both CD40L and BAFF were plated at a density of 300×10^4 cells on 10 cm dish and were cultured overnight at 37 °C with 5% CO_2 in DMEM supplemented with 10% FBS and and 1× penicillin/streptomycin. After culture, cells were treated with 10 μg/mL mytomycin C (HY-13316, MCE) for 2–3 h at 37 °C. The cells were wash with PBS and were cultured in complete RPMI-1640 medium with 1 ng/mL IL-4 (214-14, peprotech) for preparation. B cells were isolated by negative selection as described above, and were seeded at a density of 75×10^4 cells on 40LB feeder in prepared 10 cm dish. The expanded B cells collected from the suspension were analyzed by flow cytometry on day 4. For plasma cell differentiation, 15×10^4 B cells from day 4 were replated on freshly mytomycin C treated 40LB feeder cells in the presence of 10 ng/mL IL-21 (210-21, Peprotech). Cells were analyzed after 3 days of IL-21 treatment.

J_H4 intron SHM analysis

Library preparation and data analysis for the J_H4 region were performed as previously described[32,74]. In brief, GCB cells ($B220^+CD95^+GL7^+$) were sorted from the spleen of NP-KLH/MnJ-immunized mice. The genomic DNA from 1×10^5 to 2×10^5 cells was extracted using chloroform extraction and precipitated with ethanol. About 200 ng of DNA was used as input, J_H4 intron were PCR amplified with the indicated primers and the ~1.2 kb J_H4 fragments were gel-purified. The PCR products were further tagged with illumine P5 and P7 index primers and subjected to 150 bp paired-end sequencing on the DNBSEQ-T7 platform. Primers used for sequence amplification of J_H4 region are listed in Supplementary Table 1.

Data were analyzed based on the existing SHM pipeline. The raw reads were mapped to the mouse genome mm10/GRCm38 using Bowtie2 (version 2.3.5.1). The reference amplicon sequence is located on chromosome 12, from position 113,428,293 to 113,428,491, and then substitutions/deletions/insertions were called with the SAM file. The SHM pipeline reports the mutation frequency of each nucleotide. Inside the sequenced region, all sites were used for mutation spectrum analysis.

RNA-sequencing and analysis

Total RNA extraction and purification were performed using Trizol and chloroform. RNA integrity was verified using the Qsep1 Bio-Fragment Analyzer fully automated nucleic acid and protein analysis system. Purified RNA (100 ng) was subsequently utilized to prepare RNA-sequencing libraries with the VAHTS Universal V8 RNA-seq Library Prep Kit for Illumina kit (NR605-02, Vazyme) with dNTP standard method according to the provided protocol. Barcoded libraries were pooled and sequenced on the DNBSEQ-T7 platform with 150 bp paired-end reads. The Bioptic Qsep1 Bio-Fragment Analyzer fully automated nucleic acid and protein analysis system was used for quality control of library size.

RNA-seq was performed using biological replicates for all samples. Trim Galore (version 20.04.6) was used for adapter trimming of raw data, while FastQC (version 0.11.9) and MultiQC (version 1.12) were employed to assess sequencing quality. The clean reads were mapped to the mouse genome mm10/GRCm38 using Hisat2 (version 2.1.0). Differential gene expression analysis of raw featurecounts was performed using R package DESeq2. Sorted BAM files were generated using samtools (version 1.10.2) and then density bigWig files were generated by using the deepTools (version 3.5.1) with a normalizing scale factor to calculate RPKM. IGV (version 2.18.2) was used to display specialized features among genomic regions with BigWig files as the input. The heatmap and volcano map were drawn using the R package ggplot2. The inflammatory response-related pathways were obtained from the GSEA website (https://www.gsea-msigdb.org/gsea/msigdb/index.jsp) and analyzed using GSEA software (version 4.3.2). FDR.q < 0.25 in GSEA analysis is considered to indicate significant enrichment in the pathway. The GO pathway enrichment analysis of DEGs was performed using Metascape (https://metascape.org).

CUT&Tag and analysis

CUT&Tag was conducted as previously described[75]. The initial input of 1×10^5 fresh cells was bound to activated Concanavalin A beads (BP531, Bang Laboratories), and incubated with 0.5 μl anti-H3K4me3 antibody (1/100 dilution, 07-473, Millipore), 0.5 μl anti-H3K27me3 antibody (1/100 dilution, 9733, Cell Signaling Technology) or 0.5 μl Pol II antibody (1/100 dilution, 2629T, Cell Signaling Technology) for 2 h at room temperature with rotation, 0.5 μl anti-rabbit IgG antibody (1/100 dilution, ABIN101961, Antibodies Online) were performed sequentially for 1 h at room temperature with rotation, then cells were washed three times with 500 μl Dig wash buffer, next 0.5 μl Hyperactive pA-Tn5 Transposase (1/100 dilution, S603, Vazyme) were added and incubated for 1 h. Afterwards, the sample was washed three times with 500 μl of Dig-300 wash buffer, and 300 μl of tagmentation buffer was used for pA-Tn5 activation, the reaction products were subsequently subjected to DNA extraction. After PCR amplification was performed using the primers listed in Supplementary Table 1, libraries were purified with 1.3× DNA clean beads (N411, Vazyme) to get fragments larger than 250 bp. Barcoded libraries were pooled and sequenced on the DNBSEQ-T7 platform with 150 bp paired-end reads.

Trim Galore was used for adapter trimming of raw data. Alignments against the mm10 reference genome using BWA (version 0.7.17) and sorted BAM files were generated using samtools. All peaks were called using MACS3 with p-values < 1e−5. We used the broad-peak function for a definition of broad peaks. The multiBigwigSummary feature of deepTools was used to calculate the RPKM values of H3K4me3 peaks for individual genes. The density bigWig files were generated by using the deeptTools with a normalizing scale factor to

calculate RPKM values. IGV was used to display specialized features among genomic regions with BigWig files as the input. R package DiffBind was used for calculating differential peaks, and R package ChipSeeker was employed for annotating the peaks.

H3K4me3 broad peak calling and Pol II pausing index

To assess enrichments for specific protein binding to the top 5% broadest H3K4me3 domains compared to the rest of the H3K4me3 domain breadth distribution[38], the top 5% of peaks in the control group were defined as broad peaks. These broad peaks had widths greater than 5.5 kb and numbered 568 peaks. Subsequently, random sampling was performed on the remaining non-top 5% peaks to obtain a set with the same number as the top 5% peaks, which was designated as the random group. We confirmed that defining broad peaks as the top 5% widest H3K4me3 peaks is valid, as this cutoff aligns with the inflection point in the peak width distribution where peak width growth transitions to near-exponential expansion (Fig. S8), supporting the use of the top 5% as the definition for broad peaks.

Pol II pausing index calculation analysis was performed as previously described[21]. In brief, Pol II density (RPKM) were mapped within the proximal promoter (−200 bp; +200 bp with respect to TSS) and the gene body (+400 bp from TSS; TES). The Pol II pausing index was calculated using the ratio of Pol II density in the region (TSS ± 200 bp) to that in the gene body. Genes shorter than 400 bp were excluded from the pausing index analysis.

Chromatin Immunoprecipitation (ChIP)

ChIP assays were performed using the Sonication ChIP Kit (RK20258, ABclonal) according to the manufacturer's protocol with minor modifications. Briefly, 500×10^4 iGCB cells (B cells from 4 days of 40LB and IL-4 stimulation) were cross-linked with 1% formaldehyde for 10 min at room temperature and then quenched with glycine at a final concentration of 125 mM. After two washes with cold PBS, the cell pellets were frozen with liquid nitrogen and stored at −80 °C overnight. The crosslinked cells were lysed in 200 µl of Cell Swelling Buffer and then digested with 1.6 U of MNase (EN0181, Thermo Scientific) per 100×10^4 cells in 30 µl of 1 × MNase reaction buffer (B0247SVIAL, New England Biolabs). The digestion was stopped by adding 10 µl of 0.5 M EDTA (pH8.0). The nuclei ware resuspended in 500 µl of ChIP Sonication Buffer and sonicated using a VCX 130 sonicator (Sonics) with a 3 mm microtip probe to release chromatin and collect 300–500 bp fragments. 2.5% of samples was used as input and the remainder was incubated with 5 µl of anti-CGBP (1/100 dilution, ab198977, Abcam) antibodies at 4 °C for 3 h, followed by incubated with 30 µl of Protein A/G Magnetic Beads (HY-K0202, MedChemExpress) at 4 °C for 2 h. After incubation, the beads were washed sequentially with low salt wash buffer, high salt wash buffer, LiCl wash buffer and 1× TE buffer. Immunoprecipitation (IP) DNA was de-crosslinked and purified using phenolchloroform. For ChIP-seq, libraries were prepared using VAHTS Universal DNA library prep kit for Illumina (ND607, Vazyme) according to the manufacturer's instructions. Prepared libraries were sequenced on the DNBSEQ-T7 platform with 150 bp paired-end reads.

CFP1 peaks were identified using MACS3 with p-values < 1e−5, and the input background was subtracted. Other analyses were performed as described in the CUT&Tag section.

Chromosome conformation capture by 4C-HTGTS and 3C

4C-HTGTS were performed as previously described[76]. In brief, at least 1.5×10^5 cells were collected and were crosslinked with 2% formaldehyde for 10 min at room temperature and quenched with glycine at a final concentration of 125 mM. Then, the crosslinked cells were lysed in the 4C lysis buffer (10 mM Tris-HCl pH 8.0, 10 mM NaCl, 0.2 % NP-40, 1 × protease inhibitors) and nuclei were digested with 9 µl NlaIII enzyme (10,000 units/ml, R0125L, NEB) in Digestion Mix buffer (0.29% SDS, 1 × CutSmart Buffer) at 37 °C for at least two hours. Subsequently, added 16 µl of 20% Triton X-100 (220525, Amresco) and shake for 1 h at 37 °C. Next, 7 µl of NlaIII enzyme was supplemented to the reaction mixture and incubated at 37 °C overnight, and then 100 U T4 ligase was added (EL0011, Thermo) and they were incubated overnight at 16 °C. The ligated products were de-crosslinked with 40 µg Proteinase K (DE102, Vazyme) at 65 °C overnight, Subsequently, DNA was purified using phenol-chloroform extraction. The Qsep1 Bio-Fragment Analyzer detected over 80% of the DNA fragments are concentrated at sizes greater than 15 kb. The 4C-HTGTS libraries with *BCL6* promoter baits were constructed[77,78]. In brief, biotinylated PCR products amplified by LAM-PCR of sonicated DNA fragments with biotin primer were enriched with Dynabeads MyOne Streptavidin C1 beads (Invitrogen, 65002), followed by bridge adaptor ligation. The ligated products were amplified by nested PCR using barcode primers, followed by a third round of PCR using P5-I5 and P7-I7 primers. Primers used for 4C-HTGTS are listed in Supplementary Table 1.

The 4C-HTGTS libraries were then sequenced by paired-end 150 bp sequencing on the DNBSEQ-T7 platform. Data were aligned to the mm9 genome. The libraries were normalized randomly selecting the number of junctions at bait loci to match the smallest library in each set. BEDTools (version 2.27.1) was used to convert junction coordinates to bedGraph format for visualization in IGV. To enable joint visualization with other sequencing datasets across genome versions, the UCSC LiftOver tool was used to convert mm9 coordinate positions to mm10. For statistical analyses, we quantified the number of junctions at the indicated bait-interacting loci to calculate the percentage of these junctions relative to the total number of genomic junctions. The chromosome region mm9 chr16: 24,132,522-24,174,993 was defined as *Bcl6* enhancer 1, and the region mm9 chr16: 24,176,502-24,213,494 was defined as *Bcl6* enhancer 2. 3C DNA templates were generated through NlaIII restriction digestion as previously reported[79]. Quantitative PCR (qPCR) with SYBR Green was performed on 30 ng of 3C DNA using primers specified in Supplementary Table 1 to assess 3C enrichment. Interaction frequencies were normalized relative to the *GAPDH* locus to ensure comparability across samples[80].

Statistics

Except when noted otherwise, statistical analysis was performed with a two-tailed unpaired Student's t-test using Graphpad Prism software (version 9.0.0). The specific statistical test used in each case is indicated in corresponding figure legends. P-values < 0.05 were considered significant.

Reporting summary

Further information on research design is available in the Nature Portfolio Reporting Summary linked to this article.

Data availability

Previously published datasets used in this study under accession numbers GSE29282, GSE60927 and SRP048895. Our Data from RNA-seq and H3K4me3 CUT&Tag have been deposited in NCBI GEO under the accession code GSE288059, Data from Pol II & H3K27me3 CUT&Tag and CFP1 ChIP-seq have been deposited under the accession code PRJNA1283973 and PRJNA1273711, and data from SHM of J_H4 intron and 4C-HTGTS are available under the accession code PRJNA1187686. The remaining data are available within the article, Supplementary Information or Source Data file. Source data are provided with this paper.

References

1. Mesin, L., Ersching, J. & Victora, G. D. Germinal Center B Cell Dynamics. *Immunity* **45**, 471–482 (2016).
2. Victora, G. D. & Nussenzweig, M. C. Germinal centers. *Annu. Rev. Immunol.* **40**, 413–442 (2022).

3. De Silva, N. S. & Klein, U. Dynamics of B cells in germinal centres. *Nat. Rev. Immunol.* **15**, 137–148 (2015).
4. Finkin, S. et al. Protein amounts of the MYC transcription factor determine germinal center B cell division capacity. *Immunity* **51**, 324–336.e325 (2019).
5. Dominguez-Sola, D. et al. The proto-oncogene MYC is required for selection in the germinal center and cyclic reentry. *Nat. Immunol.* **13**, 1083–1091 (2012).
6. Calado, D. P. et al. The cell-cycle regulator c-Myc is essential for the formation and maintenance of germinal centers. *Nat. Immunol.* **13**, 1092–1100 (2012).
7. Ersching, J. et al. Germinal center selection and affinity maturation require dynamic regulation of mTORC1 kinase. *Immunity* **46**, 1045–1058.e1046 (2017).
8. Linterman, M. A. et al. IL-21 acts directly on B cells to regulate Bcl-6 expression and germinal center responses. *J. Exp. Med.* **207**, 353–363 (2010).
9. Weinstein, J. S. et al. TFH cells progressively differentiate to regulate the germinal center response. *Nat. Immunol.* **17**, 1197–1205 (2016).
10. Basso, K. & Dalla-Favera, R. Roles of BCL6 in normal and transformed germinal center B cells. *Immunol. Rev.* **247**, 172–183 (2012).
11. Saito, M. et al. A signaling pathway mediating downregulation of BCL6 in germinal center B cells is blocked by BCL6 gene alterations in B cell lymphoma. *Cancer Cell* **12**, 280–292 (2007).
12. Laidlaw, B. J. et al. The transcription factor Hhex cooperates with the corepressor Tle3 to promote memory B cell development. *Nat. Immunol.* **21**, 1082–1093 (2020).
13. Huang, C. et al. The BCL6 RD2 domain governs commitment of activated B cells to form germinal centers. *Cell. Rep.* **8**, 1497–1508 (2014).
14. Basso, K. & Dalla-Favera, R. Germinal centres and B cell lymphomagenesis. *Nat. Rev. Immunol.* **15**, 172–184 (2015).
15. Ochiai, K. et al. Transcriptional regulation of germinal center B and plasma cell fates by dynamical control of IRF4. *Immunity* **38**, 918–929 (2013).
16. Howe, F. S., Fischl, H., Murray, S. C. & Mellor, J. Is H3K4me3 instructive for transcription activation?. *Bioessays* **39**, 1–12 (2017).
17. Shilatifard, A. The COMPASS family of histone H3K4 methylases: mechanisms of regulation in development and disease pathogenesis. *Annu. Rev. Biochem.* **81**, 65–95 (2012).
18. Clouaire, T. et al. Cfp1 integrates both CpG content and gene activity for accurate H3K4me3 deposition in embryonic stem cells. *Genes Dev.* **26**, 1714–1728 (2012).
19. Brown, D. A. et al. The SET1 complex selects actively transcribed target genes via multivalent interaction with CpG island chromatin. *Cell Rep.* **20**, 2313–2327 (2017).
20. Thomson, J. P. et al. CpG islands influence chromatin structure via the CpG-binding protein Cfp1. *Nature* **464**, 1082–1086 (2010).
21. Chen, K. et al. Broad H3K4me3 is associated with increased transcription elongation and enhancer activity at tumor-suppressor genes. *Nat. Genet.* **47**, 1149–1157 (2015).
22. Sha, Q. Q. et al. CFP1 coordinates histone H3 lysine-4 trimethylation and meiotic cell cycle progression in mouse oocytes. *Nat. Commun.* **9**, 3477 (2018).
23. Zhang, Y. et al. Unique patterns of H3K4me3 and H3K27me3 in 2-cell-like embryonic stem cells. *Stem Cell Rep.* **16**, 458–469 (2021).
24. Cao, W. et al. CXXC finger protein 1 is critical for T-cell intrathymic development through regulating H3K4 trimethylation. *Nat. Commun.* **7**, 11687 (2016).
25. Kraus, M., Alimzhanov, M. B., Rajewsky, N. & Rajewsky, K. Survival of resting mature B lymphocytes depends on BCR signaling via the Igalpha/beta heterodimer. *Cell* **117**, 787–800 (2004).
26. Wang, C. et al. Manganese increases the sensitivity of the cGAS-STING pathway for double-stranded DNA and is required for the host defense against DNA viruses. *Immunity* **48**, 675–687.e677 (2018).
27. Lee, M. S. J. et al. B cell-intrinsic TBK1 is essential for germinal center formation during infection and vaccination in mice. *J. Exp. Med.* **219**, e20211336 (2022).
28. Taylor, J. J., Pape, K. A. & Jenkins, M. K. A germinal center-independent pathway generates unswitched memory B cells early in the primary response. *J. Exp. Med.* **209**, 597–606 (2012).
29. Nojima, T. et al. In-vitro derived germinal centre B cells differentially generate memory B or plasma cells in vivo. *Nat. Commun.* **2**, 465 (2011).
30. Kwon, K. et al. Instructive role of the transcription factor E2A in early B lymphopoiesis and germinal center B cell development. *Immunity* **28**, 751–762 (2008).
31. Laidlaw, B. J. et al. The Eph-related tyrosine kinase ligand Ephrin-B1 marks germinal center and memory precursor B cells. *J. Exp. Med.* **214**, 639–649 (2017).
32. Yeap, L. S. et al. Sequence-intrinsic mechanisms that target AID mutational outcomes on antibody genes. *Cell* **163**, 1124–1137 (2015).
33. Kundaje, A. et al. Integrative analysis of 111 reference human epigenomes. *Nature* **518**, 317–330 (2015).
34. Ernst, J. & Kellis, M. ChromHMM: automating chromatin-state discovery and characterization. *Nat. Method.* **9**, 215–216 (2012).
35. Béguelin, W. et al. EZH2 is required for germinal center formation and somatic EZH2 mutations promote lymphoid transformation. *Cancer Cell* **23**, 677–692 (2013).
36. Lin, Z. et al. SETD1B-mediated broad H3K4me3 controls proper temporal patterns of gene expression critical for spermatid development. *Cell Res.* **35**, 345–361 (2025).
37. Sze, C. C. et al. Coordinated regulation of cellular identity-associated H3K4me3 breadth by the COMPASS family. *Sci. Adv.* **6**, eaaz4764 (2020).
38. Benayoun, B. A. et al. H3K4me3 breadth is linked to cell identity and transcriptional consistency. *Cell* **163**, 1281–1286 (2015).
39. Coleman, T. R. The 3 Rs of Cdc6: recruitment, regulation, and replication. *Curr. Biol.* **12**, R759 (2002).
40. Muramatsu, M. et al. Class switch recombination and hypermutation require activation-induced cytidine deaminase (AID), a potential RNA editing enzyme. *Cell* **102**, 553–563 (2000).
41. Schwab, S. R. & Cyster, J. G. Finding a way out: lymphocyte egress from lymphoid organs. *Nat. Immunol.* **8**, 1295–1301 (2007).
42. Abraham, A. et al. Arid1a-dependent canonical BAF complex suppresses inflammatory programs to drive efficient germinal center B cell responses. *Nat. Immunol.* **25**, 1704–1717 (2024).
43. Subramanian, A. et al. Gene set enrichment analysis: a knowledge-based approach for interpreting genome-wide expression profiles. *Proc. Natl Acad. Sci. USA* **102**, 15545–15550 (2005).
44. Fukuda, T. et al. Disruption of the Bcl6 gene results in an impaired germinal center formation. *J. Exp. Med.* **186**, 439–448 (1997).
45. Basso, K. et al. Integrated biochemical and computational approach identifies BCL6 direct target genes controlling multiple pathways in normal germinal center B cells. *Blood* **115**, 975–984 (2010).
46. Hatzi, K. et al. A Hybrid mechanism of action for BCL6 in B cells defined by formation of functionally distinct complexes at enhancers and promoters. *Cell Rep.* **4**, 578–588 (2013).
47. Avery, D. T. et al. B cell-intrinsic signaling through IL-21 receptor and STAT3 is required for establishing long-lived antibody responses in humans. *J. Exp. Med.* **207**, 155–171 (2010).
48. Chu, C.-S. et al. Unique immune cell coactivators specify locus control region function and cell stage. *Mol. Cell* **80**, 845–861.e810 (2020).
49. Ying, C. Y. et al. MEF2B mutations lead to deregulated expression of the oncogene BCL6 in diffuse large B cell lymphoma. *Nat. Immunol.* **14**, 1084–1092 (2013).

50. Zotos, D. et al. IL-21 regulates germinal center B cell differentiation and proliferation through a B cell-intrinsic mechanism. *J. Exp. Med.* **207**, 365–378 (2010).
51. Haniuda, K., Fukao, S. & Kitamura, D. Metabolic reprogramming induces germinal center B cell differentiation through Bcl6 locus remodeling. *Cell Rep.* **33**, 108333 (2020).
52. Ci, W. et al. The BCL6 transcriptional program features repression of multiple oncogenes in primary B cells and is deregulated in DLBCL. *Blood* **113**, 5536–5548 (2009).
53. Cyster, J. G. & Allen, C. D. C. B cell responses: cell interaction dynamics and decisions. *Cell* **177**, 524–540 (2019).
54. Elsner, R. A. & Shlomchik, M. J. Germinal center and extrafollicular B cell responses in vaccination, immunity, and autoimmunity. *Immunity* **53**, 1136–1150 (2020).
55. Ise, W. et al. T follicular helper cell-germinal center b cell interaction strength regulates entry into plasma cell or recycling germinal center cell fate. *Immunity* **48**, 702–715.e704 (2018).
56. Litzler, L.C. et al. Protein arginine methyltransferase 1 regulates B cell fate after positive selection in the germinal center in mice. *J. Exp. Med.* **220**, e20220381 (2023).
57. Suan, D. et al. CCR6 defines memory B cell precursors in mouse and human germinal centers, revealing light-zone location and predominant low antigen affinity. *Immunity* **47**, 1142–1153.e1144 (2017).
58. Wang, Y. et al. Germinal-center development of memory B cells driven by IL-9 from follicular helper T cells. *Nat. Immunol.* **18**, 921–930 (2017).
59. Zuccarino-Catania, G. V. et al. CD80 and PD-L2 define functionally distinct memory B cell subsets that are independent of antibody isotype. *Nat. Immunol.* **15**, 631–637 (2014).
60. Luo, X. et al. An interleukin-9-ZBTB18 axis promotes germinal center development of memory B cells. *Immunity* **58**, 861–874.e866 (2025).
61. Cousu, C. et al. Germinal center output is sustained by HELLS-dependent DNA-methylation-maintenance in B cells. *Nat. Commun.* **14**, 5695 (2023).
62. Caganova, M. et al. Germinal center dysregulation by histone methyltransferase EZH2 promotes lymphomagenesis. *J. Clin. Invest.* **123**, 5009–5022 (2013).
63. Velichutina, I. et al. EZH2-mediated epigenetic silencing in germinal center B cells contributes to proliferation and lymphomagenesis. *Blood* **116**, 5247–5255 (2010).
64. Yu, C. et al. CFP1 regulates histone H3K4 trimethylation and developmental potential in mouse oocytes. *Cell Rep.* **20**, 1161–1172 (2017).
65. Jiang, Y. et al. CXXC finger protein 1-mediated histone H3 lysine-4 trimethylation is essential for proper meiotic crossover formation in mice. *Development* **147**, dev183764 (2020).
66. Andreu-Vieyra, C.V. et al. MLL2 is required in oocytes for bulk histone 3 lysine 4 trimethylation and transcriptional silencing. *PLoS Biol.* **8**, e1000453 (2010).
67. Glaser, S. et al. Multiple epigenetic maintenance factors implicated by the loss of Mll2 in mouse development. *Development* **133**, 1423–1432 (2006).
68. Sha, Q. Q. et al. Role of CxxC-finger protein 1 in establishing mouse oocyte epigenetic landscapes. *Nucleic Acids Res.* **49**, 2569–2582 (2021).
69. Margaritis, T. et al. Two distinct repressive mechanisms for histone 3 lysine 4 methylation through promoting 3′-end antisense transcription. *PLoS Genet.* **8**, e1002952 (2012).
70. Hu, S. et al. H3K4me2/3 modulate the stability of RNA polymerase II pausing. *Cell Res.* **33**, 403–406 (2023).
71. Wang, H. et al. H3K4me3 regulates RNA polymerase II promoter-proximal pause-release. *Nature* **615**, 339–348 (2023).
72. Hu, D. et al. The Mll2 branch of the COMPASS family regulates bivalent promoters in mouse embryonic stem cells. *Nat. Struct. Mol. Biol.* **20**, 1093–1097 (2013).
73. Denissov, S. et al. Mll2 is required for H3K4 trimethylation on bivalent promoters in embryonic stem cells, whereas Mll1 is redundant. *Development* **141**, 526–537 (2014).
74. Yang, D. et al. REV7 is required for processing AID initiated DNA lesions in activated B cells. *Nat. Commun.* **11**, 2812 (2020).
75. Kaya-Okur, H. S. et al. CUT&Tag for efficient epigenomic profiling of small samples and single cells. *Nat. Commun.* **10**, 1930 (2019).
76. Oudelaar, A.M., Downes, D.J., Davies, J.O.J. & Hughes, J.R. Low-input Capture-C: a chromosome conformation capture assay to analyze chromatin architecture in small numbers of cells. *Biol. Protoc.* **7**, e2645 (2017).
77. Zhao, B. et al. USP7 promotes IgA class switching through stabilizing RUNX3 for germline transcription activation. *Cell Rep.* **43**, 114194 (2024).
78. Hu, J. et al. Detecting DNA double-stranded breaks in mammalian genomes by linear amplification-mediated high-throughput genome-wide translocation sequencing. *Nat. Protoc.* **11**, 853–871 (2016).
79. Bunting, K. L. et al. Multi-tiered reorganization of the genome during B cell affinity maturation anchored by a germinal center-specific locus control region. *Immunity* **45**, 497–512 (2016).
80. Guo, C. et al. CTCF-binding elements mediate control of V(D)J recombination. *Nature* **477**, 424–430 (2011).
81. Meng, F. L. et al. Convergent transcription at intragenic super-enhancers targets AID-initiated genomic instability. *Cell* **159**, 1538–1548 (2014).

Acknowledgements

We thank Dr. Hai Qi for the 40LB feeder cells. This work was supported by National Natural Science Foundation of China (32070892 and 32270934 to J.D.); Sanming Project of Medicine in Shenzhen (SZSM202011004 to J.D.); Open Fund of Guangdong Provincial Key Laboratory of Digestive Cancer Research (2021B1212040006 to J.D.); the China Postdoctoral Science Foundation (2023M743995 to W.B.); the Postdoctoral Fellowship Program of CPSF (GZB20240883 to W.B.); and Guangdong Basic and Applied Basic Research Foundation (2023A1515111048 to W.B.).

Author contributions

J.D. conceived the project. J.D. and W.B. designed the experiments. Y.Z., S.G., W.B., Y.Y., Y.L., J.B., and M.L. performed the experiments. Y.Z., S.G., W.B., and J.D. analyzed the data. Y.Z., S.G., and J.D. wrote the manuscript with help from W.B. All authors participated in the discussion and helped revise the manuscript.

Competing interests

The authors declare no competing interests.

Additional information

Supplementary information The online version contains supplementary material available at https://doi.org/10.1038/s41467-025-63291-8.

Correspondence and requests for materials should be addressed to Wanyu Bai or Junchao Dong.

Peer review information *Nature Communications* thanks Jeremy Boss, David Dominguez-Sola and the other, anonymous, reviewer(s) for their contribution to the peer review of this work. A peer review file is available.